- National Technical University Of Athens
- School Of Chemical Engineering
- Joint Post-Graduate Program “Computational Mechanics”

Master Of Science Thesis

Computational Modeling Of Cancer Stem Cells In A Vascular Growing Tumor: A Two-Dimensional Continuum Level Approach

Giannakopoulos Athanasios

Supervisor: Kavousanakis Michail

Athens, 2023

Abstract

The purpose of this thesis is to provide new insight on how cancer stem cells (CSCs) affect the progression of a tumor, with the use and expansion of 2D modeling techniques, provided by Hubbard and Byrne (2012) [1]. The equations governing cancer dynamics were expanded to incorporate the existence of cancer stem cells, a type of cells whose existence has been questioned and highly researched, since the beginning of 20th Century.

Cancer stem cells, highly theorized as the main reason for metastasis, are a very resilient-to-drugs type of stem cells, which have been for the last years the subject of extended treatment breakthroughs. It is yet a not so well understood how they can be effectively killed, since their resilience to chemotherapy and radiotherapy pushes science to alternative methods of healing.

In this study, the mathematics of this resilience becomes the steppingstone for extended research of how cancer stem cells' parameters of growth and death are related to those of normal tumor cells. A set of parametric studies is performed, and a basic comparison between two models becomes the main attribute for the depiction of the CSCs-inclusive model.

Using COMSOL Multiphysics®, an Engineering software, the simulations are carried out by incorporating equations of mass, and momentum balance. A set of parameters is incorporated as well, and mainly three parameters are varied for the results: the probability of asymmetry division δ, the dimensionless growth rate of CSCs (k_{15}^{*}) and the dimensionless death rate of CSCs (k_{25}^{*}). The final results are discussed, along with some propositions for further research, and accompanying details for the extension of the modeling techniques for therapy.

Key Words: Cancer Stem Cells, Modeling, Growth Rate, Death Rate, Cells, Parametric, Vessels, Cancer, Tumor

Contents

Acknowledgements

To begin with, the purpose of this thesis is to provide useful scientific data that can help the scientific realm improve cancer research.

I want to thank all the contributors for this work, and most of all, all the researchers whose cancer modeling work, since 1997, has been the basis for this effort and all the future cancer modeling efforts. It is a collective work, and it is most of all, for patients that all the laboratories struggle to export data that may help.

I am deeply grateful to my professor, Kavousanakis Michail, who trusted me through this scientific journey, and has given me the opportunity to occupy myself with such an interesting and important topic as cancer stem cells. My thesis would not be achieved in the same way, were it not for the help as well of the PhD student of our laboratory, Lampropoulos Ioannis. I need to thank him and wish him to continue successfully his remarkable research on tumor modeling.

There are some people, for without their help I wouldn't be the same capable to achieve this thesis. I want to thank my family for supporting me through this whole scientific journey and believing in me. I also need to thank Kleidi Evridki, my hero, who inspired me to chase my dreams. I thank all my beloved friends, for without them I wouldn't be the same blessed in my life. Especially, I need to express my gratitude to Stavropoulou Maria, who holds a special place in my heart, as she is one of my friends who actively believed in me and my capabilities. Her help during the whole span of this Master program, where I met her, it has been a true blessing for me. Last but never least, is Presi Dimitra – Antonia, my lifetime best friend, who supports me in every step and every aspect of my life. She is a true guardian angel for me, and I owe her a lot.

I dedicate this thesis, to all people struggling with this obstacle named cancer in their lives. I deeply believe that science and life itself is miraculous. I truly believe that, as time goes by, cancer will be a totally curable disease. If at least one patient may benefit in the future from this thesis and all relevant future research, then my goal has been achieved. Because goals have not necessarily to do with educational ascension.

Instead, they may have to do with deeply caring for the healing of human pain, and bringing relief to families and people facing barriers they need to overcome.

1. Cells And Cancer

Cancer has been one of the most killing, as well as studied diseases of the last centuries. In the light of 2023, new therapies for cancer have shed light on what this disease is, as well as on what its underlying reasons for its origination may be. Undoubtedly, tumorigenesis can be attributed to genetic, environmental, lifestyle and psychological factors [2] which means that, a cancer-free health status must be free from several risks. For the rest of the chapter, the cell life cycle and how this cycle can be interrupted by tumorigenesis, are analyzed in detail.

1.1. Life Cycle Of A Cell

Cell Cycle is the main attribute of a cell's life, and it is divided in 2 stages: The Interphase and Mitosis. Interphase is divided into 3 sub-stages (Gap 1 - G1, Synthesis - S and Gap 2 - G2 phases), while Mitosis is divided into 4 sub-stages (Prophase, Metaphase, Anaphase, Telophase). All phases are shown in Fig. 1.1:

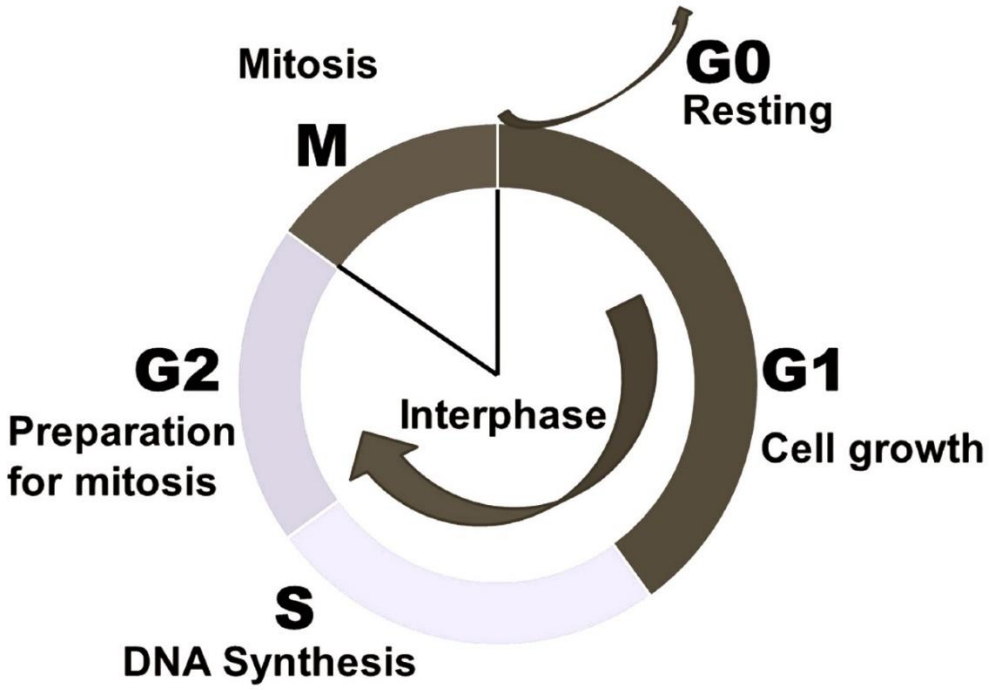

Figure 1.1: Cell Life Cycle [3]

Interphase

Interphase is the time between two successive mitosis cycles. In general, the cell prepares to become capable of division and the time needed to complete the Interphase is approximately 95% of the total cycle time [4].

a) G1 Phase (Gap 1):

When in G1 Phase, Cells increase in size, and carry out their normal metabolic function. Preparation for DNA replication happens as well. The cellular components that are needed for the subsequent division are synthesized, i.e., organelles, enzymes, proteins etc.

b) S Phase (Synthesis):

S phase is destined for DNA replication, in such a way that the 23 pairs of chromosomes are doubled in the cell and are connected to a centromere. The synthesis of DNA requires a very detailed error-correcting process, through DNA polymerase enzymes that regulate its almost-infallible division.

c) G2 Phase (Gap 2):

G2 is the phase where the cell continues to prepare for its division. DNA damage is speculated, and post-DNA replication errors are corrected. Proteins that are needed for cell division are also synthesized.

Mitotic Phase

The mitotic phase, which is destined to the chromosome separation, and lasts short compared to the Interphase. Cell growth has come to an end by this point. The division of the nucleus is followed by the division of the cytoplasm through cytokinesis. In the

end of mitosis, two daughter cells have been produced. Specifically, mitosis can be sub-classified in the following sub-phases:

a) Prophase

During Prophase, chromatin is becoming denser in its concentration, and becomes visible, even with the light microscope, as dark distinct bodies inside the cell nucleus (chromosomes) [5].

b) Metaphase

During Metaphase, the spindle fibers, which are microtubes emanating from opposite poles of the cell, they have the role of positioning the chromosomes in a specific way. The spindle fibers attach to the centromeres of the chromosome, creating tension. Consecutively, chromosomes are aligned along an imaginary plane, the metaphase plate, that runs through the center of the cell. That way, each daughter cell will receive an identical and complete set of chromosomes.

c) Anaphase

This is the phase where the sister chromatids are separated. The spindle fibers become shorter, and they pull the sister chromatids towards opposite poles of the cell, creating individual chromosomes.

d) Telophase

During this stage, the newly separated chromosomes arrive at opposite ends of the cell. Two distinct nuclei are created though the new nuclear envelops that are formed around each set of chromosomes.

G0 Phase:

There is also a distinct phase where cells enter, when they are in a quiescent state, called the G0 phase. It is not often included in the traditional descriptions of the cell cycle, as a phase where there is not active preparation for division [6]. The functions of this stage include maintenance, extended or temporary rest. When receiving signals to halt their progression, cells enter from G0 to G1 Phase.

1.2. Tumor definition and types

Tumors can be initially classified as benign and malignant. Benign tumors are a form of tumor, that simply occupies some space in the body, and stays static in its initial position. They are typically surrounded by a fibrous or connective tissue capsule that separates them from adjacent tissues. In benign tumors, the main problems are the applied pressure to an important body structure, and the over-production of hormones [7].

Malignant tumors, in contrast to benign tumors are invasive. They deplete nutrients from the body's tissues, harming their host severely. They can grow rapidly and unpredictably, and often display abnormal and irregular features, including variations in size and shape (pleomorphism) [8].

The two tumor types can have specific contradicting differences. Table 1 presents the key characteristics of a tumor formed in human breasts, depending on its type (malignant or benign) [9]:

Table 1: Key Differences Between Benign and Malignant Breast Tumor [9]

Benign Tumor	Malignant Tumor
Slow growth	Fast Growth
Capsulated	Non-Capsulated
Non-Invasive	Invasive and Infiltrate
Non-metastatic	Metastatic
Shape characterized as smooth or oval or lobulated or regular	Shape characterized as nodular or stellate or irregular
Painful	Painless
No skin dimpling	Dimpling
No nipple retraction	Nipple retraction

In Fig 1.2, sixteen mammography (X-Ray Images used for breast cancer diagnosis) images are presented, showing the morphology of the 2 tumor types.

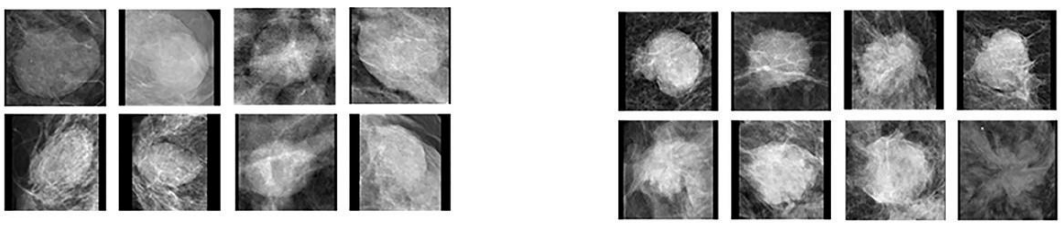

Figure 1.2 Left: Benign Breast Tumor Mammography Images, Right: Malignant Breast Tumor Mammography Images [10]

1.3. Tumorigenesis Factors

Tumorigenic factors are the factors that contribute to the genesis of a malignant tumor. Those factors include:

1. External/ environmental factors can be:
    - Ionizing and ultraviolet radiation.
    - Chemical substances, such as asbestos, tobacco smoke ingredients, aflatoxin, and heavy metals such as arsenic.
    - Biological components, i.e., infections from certain viruses, parasites and bacteria. For example, human papillomavirus (HPV) can be directly linked to tumorigenesis. It has been found that 70% of oropharyngeal cancers in the United States has been caused by HPV [11].
    - Undefined nature of particles. It has been found that PM2.5 (Particulate Matter of whichever nature, with a diameter less than 2.5 microns, are directly linked to lung cancer [12].

2. Cancer can be linked to genetic inheritance:

    Although it is not possible for cancer to be passed down as a disease itself, genetic predisposition can be inherited from parents to their offsprings. [13].

3. Psychological and psychosocial factors may also increase the risk of cancer:

Specifically, depression, anxiety and low social support may lead to increased likelihood of cancer genesis [14]. Evidence on how these two are linked are not conclusive, though it is now known that mechanisms such as endocrine reactions and inflammation are a possible connection between the two [15].

1.4. The hallmarks of cancer initiation

According to a 2000 breakthrough study by Hanahan and Weinberg [16], there are six basic stages of tumor initiation:

1. Insensitivity to anti-growth signals
2. Self-sufficiency in growth
3. Evading apoptosis
4. Sustained angiogenesis
5. Limitless replicative potential
6. Tissue invasion and metastasis

In 2011, 4 more stages were added to the hallmarks:

- Avoiding immune destruction
- Deregulating cellular energetics
- Genome instability and mutation
- Tumor-promoting inflammation

These 4 "new" hallmarks are in-between the known ones, and all hallmarks can be treated with a certain therapy, mainly inhibitors. In a more in-depth analysis, these 10 stages can be described as follows:

1. Insensitivity to anti-growth signals

Normal cells have mechanisms that prevent them from dividing unstoppably. Cancer cells tend to ignore the signals they receive to stop or slow down the division. This hallmark is often associated with activation of the onco-genes. The cells that are going to become cancerous proliferate uncontrollably in the absence of external stimuli [17].

2. Self-sufficiency in growth

The second stage is relevant to the repression of the onco-suppressing genes. Onco-suppressing genes are responsible for the suppression of the cells' accelerated division, which, here is not suppressed. Again, in the absence of external stimuli, the uncontrollable division is a malfunction of the cell's signaling system.

3. Evading Apoptosis

The natural process of programmed cell death, for the elimination of damaged or unwanted cells, it is again resisted through mechanisms developed by tumor cells.

4. Sustained Angiogenesis

The process of forming new blood vessels is greatly associated with cancer genesis. Tumors develop their own vasculature system, which enriches its system with nutrients, and thus contributes to the disanalogous development of cancer cells.

5. Limitless replicative potential

The well-known Hayflick limit [18], which implies the limited number of cell divisions, it does not apply on tumor cells. They in fact have the ability to surpass the limit indefinitely, and thus are considered immortal.

6. Tissue Invasion and Metastasis

The final hallmark of cancer is the stage of metastasis. It is thought to happen through the transport of cancer material, and especially CSCs (analyzed further below) through the blood vessels [19].

The additional hallmarks of cancer, were analyzed in 2011 by Hanahan and Weinberg [20]:

- Avoiding Immune Destruction

Cancer cells develop the ability to bypass the immune system's detection and destruction mechanisms, thus they are able to deplete the body's nutrients without provoking its reaction.

- Deregulating Cellular Energetics

As energy-demanding cells, due to their rapid and endless reproduction, cancer cells alter their energy metabolism to meet their increased demands. That is why the normal oxidative phosphorylation process is substituted by the less energy-efficient process of glycolysis.

- Genome Instability and Mutation

Cancer cells develop heterogeneity and genomic instability, and through the development of genetic mutations, they are developing resistance to therapies. Therapies are becoming less catalytic, due to the lack of homogeneity in the genome to be targeted.

- Tumor-Promoting Inflammation

Inflammation is a natural process as a response of the immune system to infections or tissue damage. Chronic inflammation though, it is associated with cancer, and oncogenesis processes like DNA damage, angiogenesis signals, remodeling of the extracellular matrix, etc. In general, tumorigenesis and inflammation are two interconnected processes, which are counter-reinforcing.

The 10 hallmarks of cancer initiation, in the order given by Hannanah and Weinber [20], are presented in Fig.1.3:

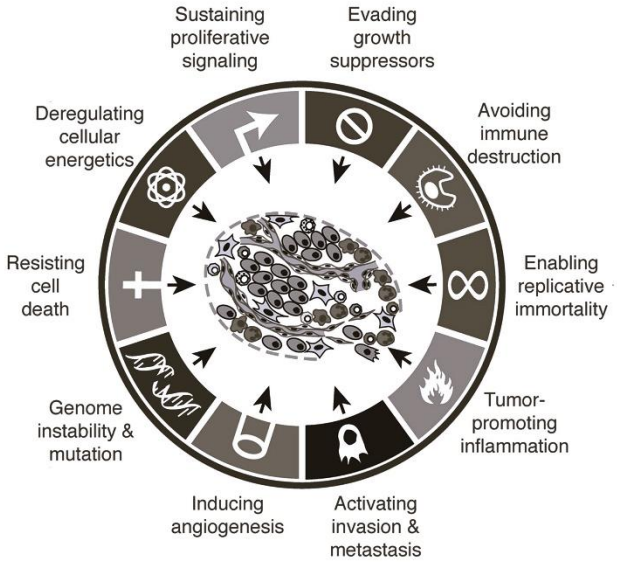

Figure 1.3: The 10 hallmarks of Cancer [15]

2. Cancer Stem Cells

2.1. Definition of Cancer Stem Cells

Cancer stem cells have been the subject of an ongoing research since early 20th Century. Their very first discovery steps began in 1937 [21]. There are two main theories explaining their existence and function. That is, the stochastic, and the hierarchical. Recently, efforts have been made to show that the two theories are interconnected [22]. Nevertheless, to this day, there is no definite proof in favor of either theory.

The discovery of cancer stem cells began with evidence of cells with stem-like properties in leukemia. Specifically, it was found that only a proportion of leukemic tumor cells can cause leukemia, when transplanted into a healthy body, which is a characteristic of their stemness [23].

Some key characteristics of CSCs are:

- Slow proliferation rates. Compared to healthy cells, they divide slower, which is a key characteristic of all stem cells.
- Slow death rates. In fact, CSCs have the immortality characteristic, which is showcased through all the therapeutic data.
- Conventional therapies, such as chemotherapy and radiotherapy, do little against CSCs. Although able to diminish their volume, most non-surgical methods cannot eliminate CSCs.
- Their existence inside a tumor is sustained through a protective environment, in which they grow, called niche [24].
- They may undergo symmetric division, as well as asymmetric division. Symmetric division is when a cancer stem cell gives two daughter CSCs, while asymmetric division produces one daughter CSC and one tumor cell. Symmetry division is expressed through its symmetry division probability δ.

- They are believed to be the main cause of metastasis. CSCs can travel throughout the body, through the vessels, and are the tumorous material that begins the growth of tumors in different regions of the body.
- They exist in varying proportions inside a tumor. It has been found that the volumetric ratio of CSCs can vary from 0,1% to 82,5% [25]. For example, in Melanoma CSCs can be at 2.5%, in Head and neck squamous cell carcinoma CSC can vary from 10 to 12%, and in Bladder cancer they can vary from 3 to 36,3% [26]
- Their therapy is believed to be most successful when their metabolic pathways are targeted. Targeting pathways like epithelial-to-mesenchymal-transition (EMT), can be one of the most beneficial treatments. Some new insights for CSCs' effective treatment are presented in Fig. 2.1.

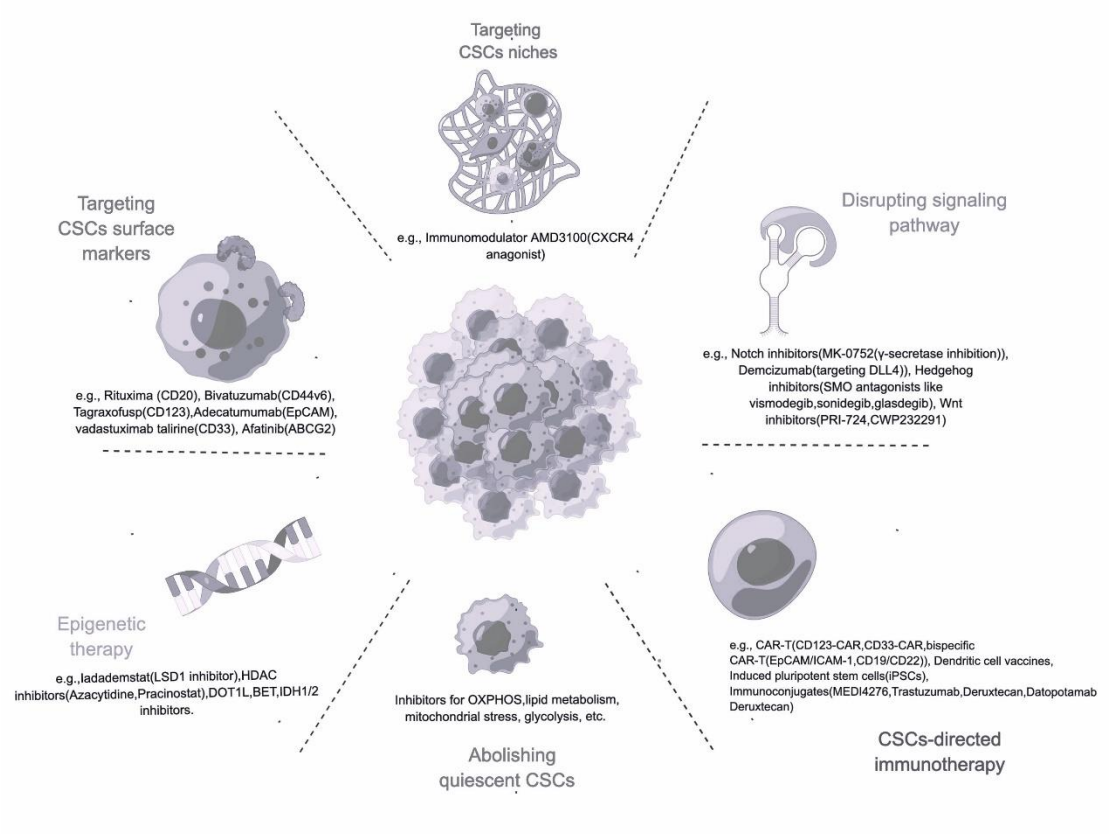

Figure 2.1: Some new insights in metabolic pathways targeted therapies for CSCs [27]

2.2. Theories on CSCs function

It must be mentioned, that for no theory there is a definite proof. The whole concept has been controversial since its beginning and the proof of CSC existence is relied only in experimental data. Cells are taken out from a tumor, and then transplanted, as it has happened since the beginning of their discovery (transplantation of leukemic cells in mice). The setback of the method is that direct evidence is needed that CSC are feeding tumor growth inside the initial body, and not the one they have been transplanted to [28].

The 2 dominant theories for CSCs function, as explained above, are the hierarchical and stochastic. A further explanation of the two, can be as below:

- According to the hierarchical model, or as named, the Cancer Stem Cell model, a tumor happens because of CSCs generated from divisions of either normal embryonic stem cells (EMCs), or progenitor cells, which can originate from birth or may be concentrated over extended time periods from cells dividing uncontrollably [29]. It essentially proposes that only cancer stem cells are the origin of cancer. The model was proposed by John Dick and colleagues in a 1994 [30].
- On the other hand, the stochastic model. or clonal evolution model (CE), was proposed in 1976 by Peter Nowell, and it essentially predicts that all undifferentiated cells can change into a tumorigenic cell.

As stated below, there is also the model that combines the two theories. It is called the plasticity model, and it proposes that cancer cells can be interlinked with stem cells and other differentiated states. It states that processes inside the tumor cells microenvironment could result in tumor cells' stem properties acquisition. There is also the ability for cancer stem cells to differentiate into non-stem tumor cells. All three models are shown in Fig.2.2.

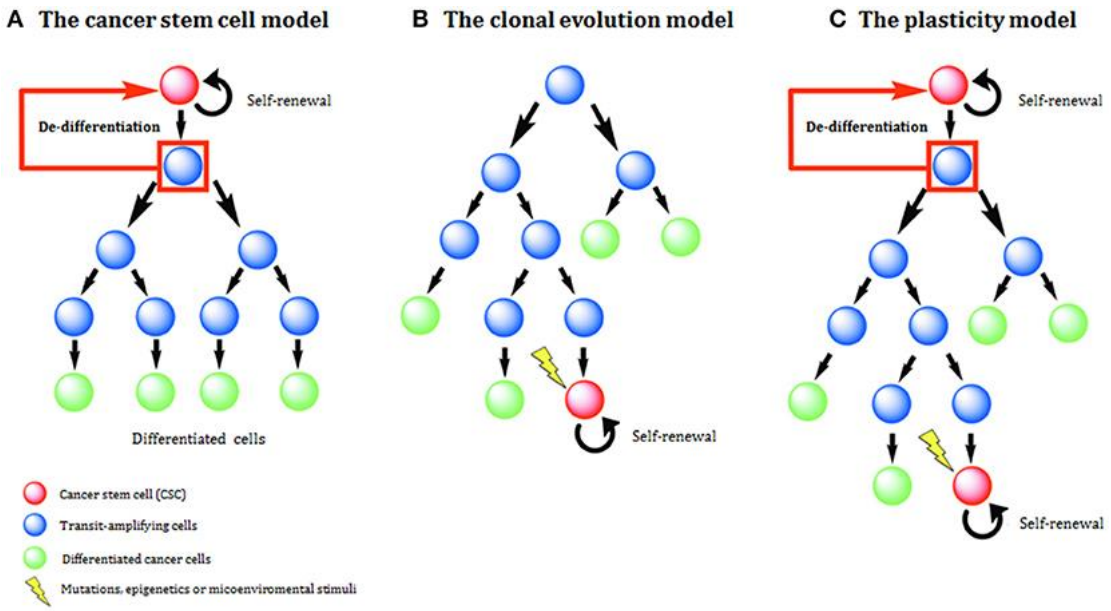

Figure 2.2: Schematic Representation of the two dominant CSC models, as well as of the hybrid one [31]

2.3. Therapeutic Data on Cancer Stem Cells

As stated above, CSCs are highly resistant to conventional therapies. It has been found that radiotherapy may be therapy-neutral to CSC, or even induce relapse and metastasis [32]. That does not mean, in any case, that conventional therapies should not be included in the treatment plan. They, instead need to be enhanced with additional therapy plans.

Current efforts have led to the following treatments for cancer stem cells:

1) Targeted therapies, using monoclonal antibodies, or small molecule inhibitors to disrupt specific signaling pathways that are overexpressed in CSCs. Antibodies targeting receptors of such signaling pathways, such as EGFR1, HER2, CD20, CEA, EpCAM and MUC1 can be an efficient form of therapy. Some of the most known CSC markers that can be targeted as well are the cell-surface extracellular material matrix CD44, the membrane protein CD133, the antigen (usually found in epithelial cancers) ESA/EpCAM. Drug resistance proteins can

be targeted as well, such as ALDH-1, as well as the proteins CD24 and CD20 [33].

2) Immunotherapy, especially by using CAR-T cells, a type of patient's T cells that are taken from the body and modified in the laboratory, so they can attack CSC. CAR stands for chimeric antigen receptor, and the use of CAR-T cells is most applied for the treatment of blood cancer [34].

3) Differentiation therapy: As called, this type of treatment targets the differentiation of CSCs into non -dangerous cells, using cell differentiation promoting drugs. Such drugs are Rho-kinase (ROCK) or megakaryoblastic leukemia 1 (MKL1) inhibitor [35].

4) Surgical methods, through the subtraction of the whole tumor, may be one of the most lifesavings for the removal of CSCs from the body.

5) The use of natural compounds has been found to be a source of bioactive compounds, targeting signaling pathways, or acting as chemo preventive agents. Such compounds can be sulforaphane, epigallocatechin-3-gallate, resveratrol, genistein, gingerol-6 and indole-3-carbinol [36].

3. Tumor Modeling

3.1. Modeling of a Tumor Basics

There are 2 basic categories of tumor simulation models, the continuum and the discrete cell-based ones. Both have their advantages and setbacks, that is why efforts have led to the adoption of hybrid models as well. In Fig. 3.1, some key characteristics of the two model categories are presented, which will be analyzed further in the rest of the chapter.

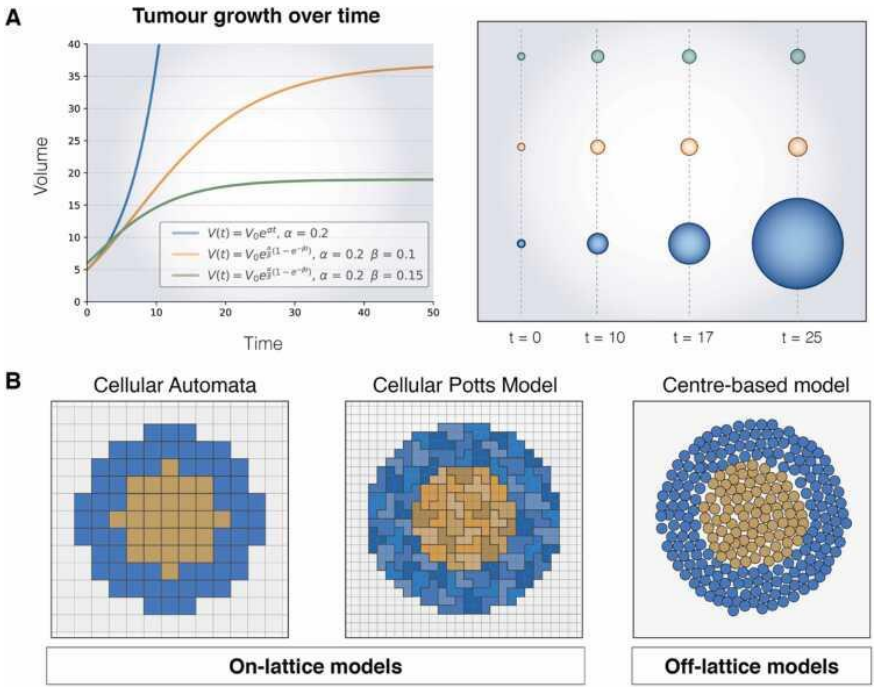

Figure 3.1: A figure showing different types of cancer simulation models. Both A diagrams show Continuum models. Section A shows the exponential Continuum model is shown in blue, and the Gompertzian in orange and green. Section B shows two lattice-based models and one lattice-free one [37]

3.1.1. Continuum Models

Continuum models, are best suited for macroscopic simulations of tumor growth. They are based on continuum mechanics, and every parameter used for the modeling is used in a deterministic approach. A considerable advantage of these models is that they do not demand high computational cost, as high as in discrete models.

Continuum models, either in 2D or 3D, are sub-classified in:

- Homogenous models
- Heterogenous models

As for homogenous models, the basic assumption is that all tumor cells are of the same form, and there is no in-depth analysis of how tumor cells populate. They are based on experimental data and equations. Some of the most known such models are the logistic and the exponential [38].

As for the heterogenous models, they are further sub-classified in two categories:

- ✓ The functional or compartment models. The basic assumption is that the different types of cells (e.g., healthy, normal tumor cells) are situated in different regions, based on the kinetics of the cells. These three different regions are [39]:
  1. the necrotic zone, where there is no sufficient nutrient and cells die.
  2. the quiescent zone, a zone where there is hypoxia and cells are in a quiescent state, and
  3. the proliferating zone, where there is rich supply of nutrient, and cells proliferate in fast paces.

- ✓ The Spatio-Temporal models. In this category lies the Hubbard and Byrne 2012 publication [1], one can find the differentiated zone models (DZM), as well as the mixed zone models (MZM).

    1. For the differentiated zone models, different cells are situated in different regions of the tumor. There is again this classification between dead, quiescent and proliferating cells.
    2. For the mixed zone models, there is no discretization between the regions of different cells. There is no specific assumption on how the tumor cells evolve, it is something that is estimated by the model progression. Ward and King's first model [40] is a mixed zone model. The same stands true for Breward, Byrne and Lewis' model in 2002 [41], and Hubbard and Byrne's model in 2012 too [1].

3.1.2. Discrete Models

As for the discrete cell-based model, the focus on the cellular phenomena and tumor microenvironment makes it an ideal simulation method, though computationally costly. Such models are classified in two sub-categories [42]:

- Lattice-based discrete models. The lattice can be structured on non-structured, and in this category belongs to the well-known Cellular Automata, where each cell depicts a single living cell. There are also the Lattice Gas Cellular Automate, where each cell depicts more than one living cell, and the Cellular Potts, where each living cell is represented by more than one cell.
  The logic of the model is that each living cell can either depart for another cell or cells' region, die, or divide and the daughter living cell occupies a new cell or cells' region.
- Lattice-free discrete models, where the interaction between the cells (represented by a single or more particles) are depicted using forces or potentials. In particular, Cell Center Modes belong in this category and the movement of each cell can be described with motion equations, as in

macroscopic physics for macroscopic bodies. Another sub-category of such models is the Boundary Tracking Models, where the cells are depicted as polygons or polyhedrons and the forces are calculated only as those who act on their edges.

In lattice-based models, the mesh (2D or 3D) is governed by deterministic or stochastic equations.

3.1.3. Hybrid Models

Hybrid models incorporate the advantages of both Continuum and Discrete models. The multi-scale simulations are based on 3 attributes [37]:

- Subcellular scale: The cell's microenvironment, as well as its signaling system are taken into consideration. Ordinary differential equations, as well as equations describing Boolean network models are used to run the simulations.
- Cellular scale: The interaction between cells, as well as between cells and extracellular material is taken into consideration. Partial differential equations and discrete models are used for the performance of simulations.
- Extracellular scale: In this sub-category, the tumor (as a whole body), and the microenvironment around it are taken into consideration for the model. Again, partial differential equations are numerically solved.

[43], [44]

3.1.4. Model Used for The Thesis

The work of this thesis was based on the MZM Continuum Model. In the direction of this effort, the beginning was made from Ward and King, and the evolution of the effort was made also by Breward et Al. in 2003 [41], who incorporated the vessels phase in the model. Hubbard and Byrne proposed in 2012 an evolved vascular model [1]. The evolution of the model has reached a stage where there is incorporation of 6 different phases inside a tumor, as in the 2022 publication from Lampropoulos, Charoupa and Kavousanakis [45]. The purpose of this thesis was to extend this model to incorporate cancer stem cells, as part of a five-phases model.

According to the model analyzed in 2012 [1], there are 4 distinct phases inside a tumor to be analyzed. That is, healthy cells, normal tumor cells, epithelial cells (vessel phase) and extracellular material. This model was further extended here, so it can incorporate a fifth phase, the cancer stem cells phase. Apart from the 5 phases, there is also the nutrient, which is the oxygen supply for the environment studied. The nutrient is delivered into the distinct phases through diffusion processes. The surface between the normal tumor cells and healthy cells is considered as a diffusive surface.

The distinct volume phases are described with the letter θ_i, where i is:

- Index 1: healthy cells,
- Index 2: normal tumor cells
- Index 3: epithelial cells (vessels)
- Index 4: extracellular material
- Index 5: cancer stem cells (CSC)

What is more, the nutrient is not considered a phase, it is described by the letter c, and here we consider only oxygen. It is diluted inside the total volume of tumorous region.

3.2. Mass Balance Equations

3.2.1. Introduction

All phases have the same, constant density. That means that the mass balance equations are applied as follows:

$$\frac{\partial \theta_i}{\partial t} + \vec{\nabla}\,(\theta_i\ \vec{u_i}) = q_i\ ,\ i = 1,\ldots,5 \qquad 3.1$$

The term $\vec{\nabla}\,(\theta_i\ \vec{u_i})$ describes the mass transfer process with convection. $\vec{u_i}$ describes the velocity of each phase θ_i, and q_i denotes the source term for each phase and describes the processes leading to mass transfer between fluid phases like:

- Cell division
- Cell death
- Angiogenesis
- Vessel occlusion

What is more, the five phases occupy a closed space, which means no mass is added or subtracted from the system. Thus, the following stands true throughout the process:

$$\sum q_i = 0 \qquad 3.2$$

We further assume that there are no voids inside the system, which is occupied completely by the 5 phases, thus:

$$\sum \theta_i = 1 \qquad 3.3$$

3.2.2. Basic model for the evolution of Healthy *a*nd *Normal* Tumor Cells

Initially, we present the original model developed by Hubbard and Byrne, which incorporates healthy, tumor cell, vessels and ECM. Then, we proceed with the

modifications we developed in order to take into account the effect of CSCs. It was assumed that all cells undergo two basic processes, proliferation (mitosis) and cell death. Growth rates are monotonically increasing with the nutrient's volumetric ratio, while death rates are monotonically decreasing with respect to the nutrient's volumetric ratio. Given the two rates described by the constant $k_{j,i}$, where j=1 denotes the growth, j=2 denotes the death rate, and i denotes the phase undergrowing death or proliferation, the following source terms describe the processes undergone by healthy and cancer cells respectively :

$$q_1 = k_{1,1}\theta_1\theta_4 \frac{c}{c_p+c} - k_{2,1}\theta_1 \frac{c_{c_1}+c}{c_{c_2}+c} \quad 3.4$$

$$q_2 = k_{1,2}\theta_2\theta_4 \frac{c}{c_p+c} - k_{2,2}\theta_2 \frac{c_{c_1}+c}{c_{c_2}+c} \quad 3.5$$

- The terms
  - ✓ $k_{1,1}\theta_1\theta_4 \frac{c}{c_p+c}$ and $k_{1,2}\theta_2\theta_4 \frac{c}{c_p+c}$ describe cell mitosis, while
  - ✓ $-k_{2,1}\theta_1 \frac{c_{c_1}+c}{c_{c_2}+c}$ and $-k_{2,2}\theta_2 \frac{c_{c_1}+c}{c_{c_2}+c}$ describe cell death,
- $\frac{c}{c_p+c}, \frac{c_{c_1}+c}{c_{c_2}+c}$ are formulated as functions of nutrient concentration c, and they obey to the following properties:
  - ✓ For the source terms: they become zero when c is zero (minimum value), and reach their maximum value, $k_{1,i}$, when c is infinite, following the Michaelis-Menden kinetics.
  - ✓ For the sink terms: the maximum value ($k_{2,I} * \frac{c_{c_1}}{c_{c_2}}$) is reached when c is zero and the minimum value is reached ($k_{2,i}$) when c reaches an infinite value.
- c_p represents the concentration of oxygen (nutrient) where there is half the maximum value of the mitosis rate. It is the same for healthy, tumor cells and CSCs (c_p = 0.25).
- c_{c1}, c_{c2} represent the threshold oxygen concentrations for cell's death rate. It is assumed that $c_{c1} > c_{c2}$, in order to apply increasing death rate as the oxygen's concentration decreases. They hold the same value for healthy, tumor cells and CSCs (c_{c1} = 0.2, c_{c2} =0.1)

- A basic hypothesis we follow in all our simulations, is that because tumor cells divide more rapidly than healthy cells, $k_{1,2} > k_{1,1}$. What is more, because, as stated below, tumorous cells have slower death rates than healthy cells, $k_{2,2} > k_{2,1}$

3.2.3. Modified Equations Incorporating Cancer Stem Cells' Equations

In this paragraph, we describe the appropriate modifications to incorporate CSCs, the θ_5 phase. For Cancer stem cells, it is proposed that the new equation follows the same pattern as that of normal tumor cells. That is because CSCs undergo cell proliferation and death, with the same evolution process as normal tumor cells, but with different parameters of growth and death rate (prescribed as k_{15} and k_{25} respectively). However, it is needed to incorporate of the asymmetry division of CSCs. That means, a percentage of CSCs gives daughter CSCs, and a percentage of CSCs gives normal tumor cells.

$$q_5 = \delta * k_{1,5}\theta_5\theta_4 \frac{c}{c_p+c} - k_{2,5}\theta_5 \frac{c_{c_1}+c}{c_{c_2}+c} \qquad 3.6$$

Where:

- δ describes the asymmetric division probability, and it varies according to the cancer type. In most cases of this thesis studied, δ was put as 0.9, which means that 90% of cancer stem cells offsprings are cancer stem cells, and 5% of CSCs offsprings are normal tumor cells.

The modified mass supply equation for normal tumor cells becomes:

$$q_2 = k_{1,2}\theta_2\theta_4 \frac{c}{c_p+c} - k_{2,2}\theta_2 \frac{c_{c_1}+c}{c_{c_2}+c} + (1 - \delta) * k_{1,5}\theta_5\theta_4 * \frac{c}{c_p+c} \qquad 3.7$$

where,

- $(1 - \delta) * k_{1,5}\theta_5\theta_4 * \frac{c}{c_p+c}$, describes the production of tumor cells originating from the asymmetric division of cancer stem cells.

For healthy cells there is no need to modify their governing mass balance equation.

3.2.4. Blood Vessel Phase (θ_3)

As for the Blood Vessels Phase (θ_3), the governing equation is:

$$q_3 = -k_3\theta_3 H(\theta_1 p_1 + \theta_2 p_2 - p_{crit}\varepsilon_3) + k_4(\theta_1 + \theta_2)\theta_3 \frac{\theta_4}{\varepsilon + \theta_4} \frac{c}{(c_a+c)^2} \quad 3.8$$

, where:

- The term $-k_3\theta_3 H(\theta_1 p_1 + \theta_2 p_2 - p_{crit}\varepsilon_3)$ denotes the vessel occlusion, and
- The term $k_4(\theta_1 + \theta_2)\theta_3 \frac{\theta_4}{\varepsilon + \theta_4} \frac{c}{(c_a+c)^2}$ denotes the angiogenesis.

A more in-depth analysis can be:

- There is monotonical increase of the supply q_3, as the volume of θ_3 phase increases. The same holds true for the total volume of the other cells (sum of θ_1, θ_2, as well as θ_5, which will be added later)
- Vessel occlusion happens as the pressure applied to the vessels by the other cells (θ_1, θ_2, as well as θ_5 which will be incorporated in the equations later) surpasses p_{crit}. Vessel occlusion gives rise to the blood flow decrease, then the shear stress reduction to the vessels, and finally regression of the vessels.
- All the other cells inside the simulated region act as angiogenic factors, while the nutrient affects the rates of angiogenesis and vessel occlusion. Maximal angiogenesis $c = c_a$, while the extremes halt the vessels' growth.
- The H term is for the Heaviside approximation function, that is calculated as:

$$H(x,k) = \frac{1}{2}\left(1 + \tanh\frac{x}{k}\right), \kappa \ll 1 \quad 3.9$$

Vessel phase is also modified in a way that is now:

$$q_3 = -k_3\theta_3 H\,(\theta_1 p_1 + \theta_2 p_2 + \theta_5 p_5 - p_{crit,}\varepsilon_3) + k_4(\theta_1 + \theta_2 + \theta_5)\theta_3 \frac{\theta_4}{\varepsilon + \theta_4} \frac{c}{(c_a + c)^2} \quad 3.10$$

3.2.5. Extracellular Material Phase (θ_4)

For the Extracellular material (ECM) phase, the modified equation (incorporating the θ_5 phase is:

$$q_4 = -k_{1,1}\theta_1\theta_4 \frac{c}{c_p + c} + k_{2,1}\theta_1 \frac{c_{c_1} + c}{c_{c_2} + c} - k_{1,2}\theta_2\theta_4 \frac{c}{c_p + c} + k_{2,2}\theta_2 \frac{c_{c_1} + c}{c_{c_2} + c} - k_3\theta_3 H\,(\theta_1 p_1 + \theta_2 p_2 + \theta_5 p_5 - p_{crit}\varepsilon_3) - k_4(\theta_1 + \theta_2 + \theta_5)\theta_3 \frac{\theta_4}{\varepsilon + \theta_4} \frac{c}{(c_a + c)^2} - k_{1,5}\theta_5\theta_4 \frac{c}{c_p + c} + k_{2,5}\theta_5 \frac{c_{c_1} + c}{c_{c_2} + c} \quad 3.11$$

, which essentially is:

$$q_4 = -q_1 - q_2 - q_3 - q_5 \quad 3.12$$

The extracellular phase essentially is what is really left of all the other materials of the simulated system, the material needed for cell growth, the apoptosis material.

Since all volumetric ratios in the system sum up to 100% of it, the following equation for the volumetric ratio of ECM holds true:

3.3. Momentum Balance Equations:

3.3.1. Governing Equations:

Conservation of momentum, assuming a flow with negligible inertial terms (lower Reynolds number), can be expressed in the following equation:

$$\vec{\nabla}\,(\theta_i * \boldsymbol{\sigma_\iota}) + \overrightarrow{F_\iota} = 0 \text{ , for i = 1, …, 5} \qquad 3.13$$

Where:

- $\overrightarrow{\sigma_\iota}$ is the stress tensor in every phase of the system, and
- $\overrightarrow{F_\iota}$ are the momentum source terms, i.e., the effects of pressure, drag force between the phases etc.

What is more:

$$\sum \nabla\,(\theta_i * \overrightarrow{u_\iota}) = 0 \qquad 3.14$$

This equation is the result of summing Eq. 3.1, to supplement Eq.3.13, and be able to calculate phase velocities $\overrightarrow{u_\iota}$.

3.3.2. Equations for the five Phases

As for the stress tensor for the five phases:

$$\boldsymbol{\sigma_\iota} = -p_i * \mathbf{I} + \mu_i * (\nabla\overrightarrow{u_\iota} + (\nabla\overrightarrow{u_\iota})^T) + \lambda_i\,(\nabla \cdot \overrightarrow{u_\iota}) * \mathbf{I}\text{, for i = 1, …, 5} \qquad 3.15$$

, where:

the letters in bold denote tensors.

- p_i stands for the pressure of phase, i.
- μ_i is the dynamic viscosity for phase, j.
- λ_i is the dynamic bulk viscosity.

- for each phase, $\lambda_\iota = -\frac{2}{3}\mu_i$, since there is thermodynamical equilibrium in all phases.

For $\overrightarrow{F_\iota}$:

$$\overrightarrow{F_\iota} = p_i \mathbf{I}\vec{\nabla}\theta_i + \sum_{j=1,j\neq 1}^{5} d_{ij}^{*}\theta_i\theta_j(\overrightarrow{u_j'} - \overrightarrow{u_\iota'}) \text{ , i=1,….,5} \qquad 3.16$$

, where d_{ij} stands for the drag coefficient concerning the relative motions of i,j phases.

What is more:

$$p_1 = p_2 = p_5 = p_4 + \Sigma(\theta) \qquad 3.17$$

where:

- θ* represents the total cell volumetric ratio ($\theta_1+\theta_2+\theta_5$). Whenever the local density of the cells surpasses θ*, the function Σ(θ) below calculates the increase in pressure.

- $\sum(\theta) = \begin{cases} \frac{\Lambda(\theta-\theta^*)}{(1-\theta)^2}, & \text{for } \theta \geq \theta^* \\ 0, & \text{for } \theta \geq \theta^* \end{cases}$ 3.18

- Λ represents the tension constant, the tendency of the cells to go back to their natural density θ* (which is prescribed later as 0.6) .

For values of density lower than θ* the cells do not interact with each other, since they are sparsely distributed. That means no relative stress is applied between them.

3.4. Reaction – Diffusion Equations for Oxygen

3.4.1. Governing Equations

Oxygen is the only diffusible species used in the simulation, since all other diffusible species' contribution is negligible. The governing equation for oxygen's diffusion is:

$$D_c \vec{\nabla}^2 c + q_c = 0 \qquad 3.19$$

, where:

- c denotes oxygen.
- $D_{c,}$ which denotes the diffusion coefficient for oxygen.
- q_c represent the net source terms for oxygen.

For $q_{c,}$ the governing equations is:

$$q_c = k_5\theta_3 (c_v - c) - k_{6,1}\theta_1 c - k_{6,2}\theta_2 c - k_{6,5}\theta_5 c - k_{7,1}\theta_1\theta_4 \frac{c}{c_p+c} - k_{7,2}\theta_2\theta_4 \frac{c}{c_p+c} - k_{7,5}\theta_5\theta_4 \frac{c}{c_p+c} \qquad 3.20$$

, where:

- The term: $k_5\theta_3 (c_v - c)$ denotes oxygen replenishment, through the vessels.
- The terms: $-(k_{6,1}\theta_1 c + k_{6,2}\theta_2 c)$ represent the baseline consumption.
- The term: $-(k_{7,1}\theta_1\theta_4 \frac{c}{c_p+c} + k_{7,2}\theta_2\theta_4 \frac{c}{c_p+c})$ denotes consumption due to cell birth.
- It is assumed that $\frac{k_{7,1}}{k_{7,2}} = \frac{k_{1,1}}{k_{1,2}}$ for consistency with the cell birth terms in Eq. 3.4 and 3.5.
- c_p is the parameter used in Eq. 3.4 and 3.5.
- c_v represents the concentration of oxygen inside the blood vessels and is assumed to be constant.

3.5. Nondimensionalization

It is convenient to rewrite the equations in dimensionless form. Volumetric ratios (θ_i) are dimensionless by nature, while $\vec{x}$, t, $\overrightarrow{u_1}$, p_i and c have to become dimensionless. That way, dimensionless variables, denoted by prime (‘), are included in the following equations:

$$t = \frac{t'}{k_{1,1}}$$
$$\vec{x} = L_o \vec{x}'$$
$$\overrightarrow{u_1} = L_o k_{1,1} \overrightarrow{u_1}'$$
$$p_i = \Lambda p_i'$$
$$c = c_v\, c'$$

3.21

, where L_o denotes a typical length scale, defined as the initial radius of the tumor, and c_v denotes the assumed constant concentration of oxygen in the blood vessels.

3.5.1. Mass Balance Equations

The nondimensionalization of the variables above, leads to the following equations for the calculation of volumetric ratios of the cells simulated inside the tumor:

- For healthy cells:

$$\frac{\partial \theta_1}{\partial t'} + \nabla' * \left(\theta_1 \overrightarrow{u_1}' \right) = \theta_1 \theta_4 \frac{c'}{c_p{}^* + c'} - k_{2,1}^* \theta_1 \frac{c_{c1+}^* c'}{c_{c2+}^* c'} \qquad 3.22$$

- For normal tumor cells:

$$\frac{\partial \theta_2}{\partial t'} + \nabla' * \left(\theta_2 \overrightarrow{u_2'} \right) = k_{1,2}^* \theta_2 \theta_4 \frac{c'}{c_p{}^* + c'} - k_{2,2}^* \theta_2 \frac{c_{c1+}^* c'}{c_{c2+}^* c'} + (1-\delta) k_{1,5}^* \theta_5 \theta_4 \quad 3.23$$

- For the blood vessels phase:

$$\frac{\partial \theta_3}{\partial t'} + \nabla' * \left(\theta_3 \overrightarrow{u_3'} \right) = -k_3^* \theta_3 G \left(\theta_1 p_1' + \theta_2 p_2' + \theta_5 p_5' - p_{crit}^* \varepsilon_3^*\right) + k_4^* (\theta_1 + \theta_2 + \theta_5) \theta_3 \frac{\theta_4}{\varepsilon + \theta_4} \frac{c'}{(c_\alpha^* + c')^2} \quad 3.24$$

- For Cancer stem cells:

$$\frac{\partial \theta_5}{\partial t'} + \nabla' * \left(\theta_5 \overrightarrow{u_5'} \right) = \delta * k_{1,5}^* \theta_5 \theta_4 \frac{c'}{c_p{}^* + c'} - k_{2,5}^* \theta_5 \frac{c_{c1+}^* c'}{c_{c2+}^* c'} \quad 3.25$$

- For the Extracellular Material (ECM) phase:

$$\theta_4 = 1 - \theta_1 - \theta_2 - \theta_3 - \theta_5 \quad 3.12$$

Some definitions for the dimensionless parameters above are:

$$k_{2,1}^* = \frac{k_{2,1}}{k_{1,1}}, k_{1,2}^* = \frac{k_{1,2}}{k_{1,1}}, k_{2,2}^* = \frac{k_{2,2}}{k_{1,1}}, k_3^* = \frac{k_3}{k_{1,1}}, \; k_4^* = \frac{k_4}{c_v k_{1,1}},$$

$$k_{1,5}^* = \frac{k_{1,5}}{k_{1,1}}, k_{2,5}^* = \frac{k_{2,5}}{k_{1,1}} \quad 3.26$$

$$c_p^* = \frac{c_p}{c_v}, c_a^* = \frac{c_a}{c_v}, c_{c_1}^* = \frac{c_{c_1}}{c_v}, c_{c_1}^* = \frac{c_{c_2}}{c_v}, \quad 3.27$$

$$p_{crit}^* = \frac{p_{crit}}{\Lambda}, \varepsilon_3^* = \frac{\varepsilon_3}{\Lambda} \quad 3.28$$

3.5.2. Momentum Balance Equations

All Equations given in Chapter 3.3 are now in presented dimensionless form:

$$\sum_{j=1,j\neq 1}^{5} d_{ij}^{*}\theta_i\theta_j(\overrightarrow{u_j'} - \overrightarrow{u_\iota'}) - \theta_i\nabla'(\Lambda^{*}p_i'\mathbf{I}) + \nabla'\{\theta_i[\mu_i^{*}(\nabla\overrightarrow{u_\iota} + (\nabla\overrightarrow{u_\iota})^{T}) - \lambda_i^{*}(\nabla'\overrightarrow{u_\iota'})\mathbf{I}]\} = 0 \quad \text{for i,j = 1 , … , 5} \qquad 3.29$$

and

$$\sum_{i=1}^{4}\nabla'(\theta_i * \overrightarrow{u_\iota'}) = 0 \qquad 3.30$$

, where:

- $d_{ij}^{*} = d_{ji}^{*}$ 3.31
- $p_1' = p_2' = p_5' = p_4' + \Sigma'(\theta),\ p_3' = \frac{p_3}{\Lambda}$ 3.32
- $\Sigma'(\theta) = \frac{(\theta-\theta^{*})}{(1-\theta)^2}$, $\theta = \theta_1 + \theta_2 + \theta_5$ (total cells' volume) 3.33
- $d_{ij}^{*} = \frac{d_{ij}}{d_{12}}, \Lambda^{*} = \frac{\Lambda}{d_{12}k_{1,1}L_0^2}, \mu_i^{*} = \frac{\mu_i}{d_{12}L_0^2}, \lambda_i^{*} = \frac{\lambda_i}{d_{12}L_0^2}$ 3.34

3.5.3. Reaction – Diffusion Equations for Oxygen

The dimensionless form for the diffusion of the nutrient is:

$$D^{*}{}_c\overrightarrow{\nabla'^2}c' = \theta_3(1-c') - k_{6,1}^{*}\theta_1 c' - k_{6,2}^{*}\theta_2 c' - k_{6,5}^{*}\theta_5 c' - k_{7,1}^{*}\theta_1\theta_4\frac{c'}{c_p^{*}+c'} - k_{7,2}^{*}\theta_2\theta_4\frac{c'}{c_p^{*}+c'} - k_{7,5}^{*}\theta_5\theta_4\frac{c'}{c_p^{*}+c'} \qquad 3.35$$

, where:

- The term $\theta_3(1-c')$ denotes replenishment.
- The term $-(k_{6,1}^{*}\theta_1 c' + k_{6,2}^{*}\theta_2 c' + k_{6,5}^{*}\theta_5 c')$ denotes baseline consumption.
- The term $-(k_{7,1}^{*}\theta_1\theta_4\frac{c'}{c_p^{*}+c'} + k_{7,2}^{*}\theta_2\theta_4\frac{c'}{c_p^{*}+c'} + k_{7,5}^{*}\theta_5\theta_4\frac{c'}{c_p^{*}+c'})$ denotes consumption due to cell birth, and:

$$D_c^* = \frac{D_c}{k_5 L_0^2}\ ,\ k_{6,1}^* = \frac{k_{6,1}}{k_5}\ ,\ k_{6,2}^* = \frac{k_{6,2}}{k_5}\ ,\ k_{6,5}^* = \frac{k_{6,5}}{k_5},$$

$$k_{7,1}^* = \frac{k_{7,1}}{c_v k_5}\ ,\ k_{7,2}^* = \frac{k_{7,2}}{c_v k_5}, k_{7,5}^* = \frac{k_{7,5}}{c_v k_5} \qquad 3.36$$

The nondimensionalization parameter here is k_5^{-1}, which denotes the rate for which oxygen is transferred from blood vessels to the tissue.

3.6. Initial And Boundary Conditions

3.6.1. Initial Conditions

For the initial conditions' definition, a healthy cellular tissue was considered, which, because of homeostasis, will be in equilibrium, so: $\theta_2 = \theta_5 = 0$, and $\theta^* = 0.6$. But, $\theta^* = \theta_1 + \theta_2 + \theta_5$, so $\theta_1 = 0.6$, and based on Eq. 3.17, $p_i = 0$, for i = 1, … , 5.

As a result, $\overrightarrow{u_i} = 0$, for i = 1 , … , 5.

It will be as well, for Eq. 3.3, 3.22, 3.24, 3.35,

$$0 = \theta^* \theta_4 \frac{c}{c_p + c} - k_{2,1} \theta^* \frac{c_{c_1} + c}{c_{c_2} + c'} \qquad 3.37$$

$$0 = -k_3 \theta_3 H(-p_{crit}, \varepsilon_3) + k_4 \theta^* \theta_3 \frac{\theta_4}{\varepsilon + \theta_4} \frac{c}{(c_\alpha + c)^2} \qquad 3.38$$

$$0 = \theta_3 (1 - c) - k_{6,1} \theta_1 c - k_{7,1} \theta^* \theta_4 \frac{c}{c_p + c} \qquad 3.39$$

The parameters above were set to:

$$\theta_1 = 0.6, \theta_2 = 0.0, \theta_5 = 0.0, \theta_3 = 0.01749783, \theta_4 = 0.3825022$$

$$c = 0.2532031, p_i = 0.0, \overrightarrow{u_i} = 0.0, k_4 = 0.002944900$$

3.40

For normal tumor cells and CSCs, it was needed to seed a tumor in the center of the studied region. 80% of the total seed volumetric ratio will be normal tumor cells, while 20% will be CSCs, in such a way that:

$$\theta_2(x,y,t=0) = \begin{cases} 0.05 * \frac{4}{5}\cos^2(\frac{\pi r}{2}), \text{for } r \leq 1 \\ 0, \qquad\qquad \text{for } r > 1 \end{cases}, \tag{3.41}$$

$$\theta_5(x,y,t=0) = \begin{cases} 0.05 * \frac{1}{5}(\cos(\frac{\pi r}{2}))^2, \text{for } r \leq 1 \\ 0 \qquad\qquad , \text{for } r > 1 \end{cases} \tag{3.42}$$

, where the radius is a function of the two-dimensional coordinates:

$$r = \sqrt{x^2 + y^2} \tag{3.43}$$

It is of great interest to note that the radius is dimensionless, but a dimensionless radius of value 1 represents a seed with an initial radius of 250µm

For the initial conditions of healthy cells, it is assumed that:

$$\theta_1(x,y,0) = 0.6 - \theta_2(x,y,0) - \theta_5(x,y,0) \tag{3.44}$$

, so $\theta_1 + \theta_2 + \theta_5 = \theta^*$ is satisfied.

Eq. 3.42 was for bell-like initial distribution of the cancer stem cells model. For simplicity reasons, this initial distribution will be often called “bell”. That means CSCs are distributed inside the tumor, and the initial concentration is situated inside the center of the tumor, according to the equation.

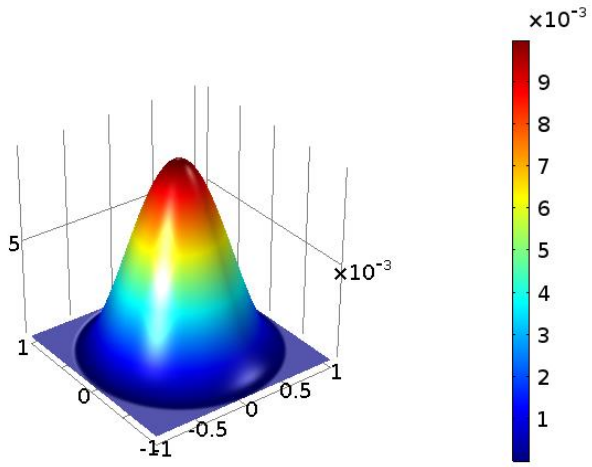

Figure 3.2: Cancer stem cells bell distribution inserted as initial conditions.

Fig.3.3. depicts the bell-like distribution for the seed containing initial concentration of CSCs. It was best decided to also simulate the initial distribution of CSCs adding some noise. Again, this CSCs' initial distribution, named Noisy Bell CSCs' initial distribution, will be often called for simplicity reasons "Noisy Bell". Its equation was chosen in a way that its initial concentration as far as possible the same with the bell CSCs' initial distribution, as shown in the Fig. 3.4.

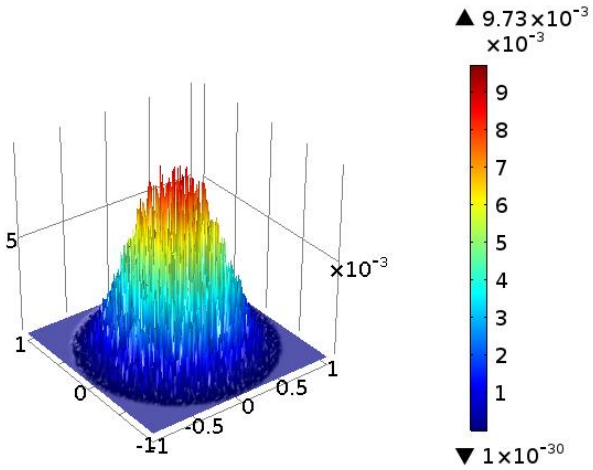

Figure 3.3: Cancer stem cells noisy bell distribution inserted as initial conditions.

For the initial concentration to be plotted in the same heights and same initial conditions, the initial CSCs distribution Equation was modified in a way that it became:

$$\theta_5(x,y,0) = \begin{cases} 2 * 0.05 * \frac{1}{5} * \text{abs}(\text{random}(x,y)) \left(\cos\left(\frac{\pi r}{2}\right)\right)^2, & r \leq 1 \\ 0, & r > 1 \end{cases} \quad 3.45$$

, where:

- abs function gives positive-only values in the distribution, and
- random(x,y) is the randomizer function of COMSOL Multiphysics® software

If the factor 2*abs were not inserted, the bell-like distribution would be equally distributed in the positive and negative values of z-axis.

As stated above, $\theta^* = \theta_1 + \theta_2 + \theta_5$ and $\theta^* = 0.6$. It is obvious, that since all the volumetric ratios sum is 1, it will be: $\theta^* + \theta_3 + \theta_4 = 1$.

3.6.2. Boundary Conditions

For the mass balance equations, which are hyperbolic, the boundary conditions imposed in the part of the simulated domain Ω boundaries ($\partial\Omega$) where there is mass inflow, are:

$$\theta_i = \theta_i(t=0), \text{ for I = 1 , … , 5} \quad 3.46$$

where:

- $\theta_i(t=0)$ is the initial volumetric ratio at the boundaries $\partial\Omega$.

In the boundary regions where there is fluid inflow, all phases are in permanent condition, and they obey the following equation:

$$\overrightarrow{u_i} * \vec{n} = 0 \quad 3.47$$

, where:

- $\vec{n}$ is the unit vector vertical to the boundary surface, pointing outwards.

For momentum balance equations, as boundary conditions in the boundaries of the domain Ω, it was imposed that:

$$\sigma_i * \vec{n} = 0 \text{ , for I = 1, 2, 3, 5} \quad 3.48$$

and

$$\overrightarrow{u_4} = 0 \text{ (which is imposed for ECM phase)} \quad 3.49$$

Eq. 3.49 is imposed as a Dirichlet Boundary condition, to obtain a unique solution.

Finally, for the nutrient's calculation equations, a Neumann boundary condition is imposed:

$$\nabla c * \vec{n} = 0 \quad 3.50$$

3.7. Parameters Used in the model

Dimensionless parameters are presented in the Table 2, provided by Hubbard and Byrne [1]:

Table 2: Dimensionless Parameters Values [1]

Dimensionless Parameter	Value	Description
$k_{1,2}^*$	2.0	Tumor cell birth rate
$k_{2,1}^*$	0.15	Healthy cell birth rate
$k_{2,2}^*$	0.075	Tumor cell death rate
k_3^*	0.1	Vessel occlusion rate
k_4^*	0.0029449	Angiogenesis rate
$k_{6,1}^*$	0.01	Nutrient consumption rate (healthy cell baseline)
$k_{6,2}^*$	0.01	Nutrient consumption rate (tumor cell baseline)
$k_{6,5}^*$	0.01	Nutrient consumption rate (CSC baseline)
$k_{7,1}^*$	0.1	Nutrient consumption rate (healthy cell birth)
$k_{7,2}^*$	$k_{7,1}^* * k_{1,2}^*$	Nutrient consumption rate (normal tumor cell birth)
$k_{7,5}^*$	$k_{7,1}^* * k_{1,2}^*$	Nutrient consumption rate (CSC birth)
c_p^*	0.25	Cell birth rate dependence on nutrient
$c_{c_1}^*, c_{c_2}^*$	0.2 , 0.1	Cell death rate dependence on nutrient
c_a^*	0.05	Angiogenesis rate dependence on nutrient

p^*_{crit}	0.3	Critical pressure for vessel occlusion
ε^*_3	0.2	Smoothness of occlusion pressure dependence
ε	0.01	Angiogenesis rate dependence on ECM
Λ^*	0.1	Cell tension constant
μ^*_i	10.0	Phase dynamic shear viscosities (i= 1, …. , N_p)
λ^*_i	$-\frac{2}{3}\mu^*_i$	Phase bulk viscosities (i= 1, … , N_p)
d^*_{ij}	1.0	Interphase drag coefficients (I, j= 1, … , N_p , j≠ i
D^*_c	1.0	Nutrient diffusion coefficient

It has to be mentioned that:

- k^*_{15} and $k^*_{25}$are a matter of research, thus parametric studies have been made here to propose the best values.
- $k^*_{1,2}$ for the two basic studies presented later, was set to 1.5 instead of 2.0, while for the parametric studies, it was set to 2.

3.8. COMSOL Multiphysics® Model

3.8.1. Some Information on the Software Solver

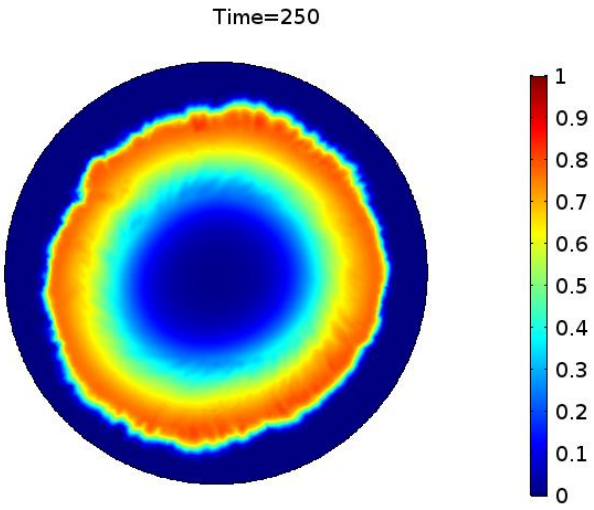

Figure 3.4: A 2D modeled tumorous circular region showing the distribution of normal tumor cells and CSCs

In Fig.3.2. a 2D simulated tumor snapshot is shown, which is modelled with the use of COMSOL Multiphysics®. COMSOL Multiphysics® is a software, which has the substantial advantage of having the ability to incorporate equations in its Finite Elements Analysis (FEA) process.

Through COMSOL Multiphysics®, MUMPS solver was used to solve the relative systems of algebraic equations. MUMPS, which stands for Multifrontal Massively Parallel sparse direct Solver. Its main attributes are:

- It is solving large linear systems with symmetric positive definite matrices, or general symmetric or general asymmetric matrices.
- It does iterative refinement and backward error analysis.
- It is written in Fortran 90.
- It does forward elimination during factorization.

[46]

Through COMSOL Multiphysics® again, BDF (Backwards Differentiation Formula) Time-Dependent Solver was used as well. It is an implicit solver, using backward differentiation methods, which are known for their stability, and have an order of accuracy ranging from one to five. It is a solver of variable order, solving with a higher order of accuracy when possible, and with a lower order, when stability is necessary to be obtained. Here, the minimum accuracy order was set to one (Backward Euler Method), and the maximum order of accuracy was set to two. [47]

For the governing equations to be inserted into the model, the equations modules were used. Specifically, for the Mass Balance equations, Transport of Diluted Species library was chosen, while for the Momentum Balance equations, Coefficient Form PDE library was chosen.

3.8.2. Mesh Information

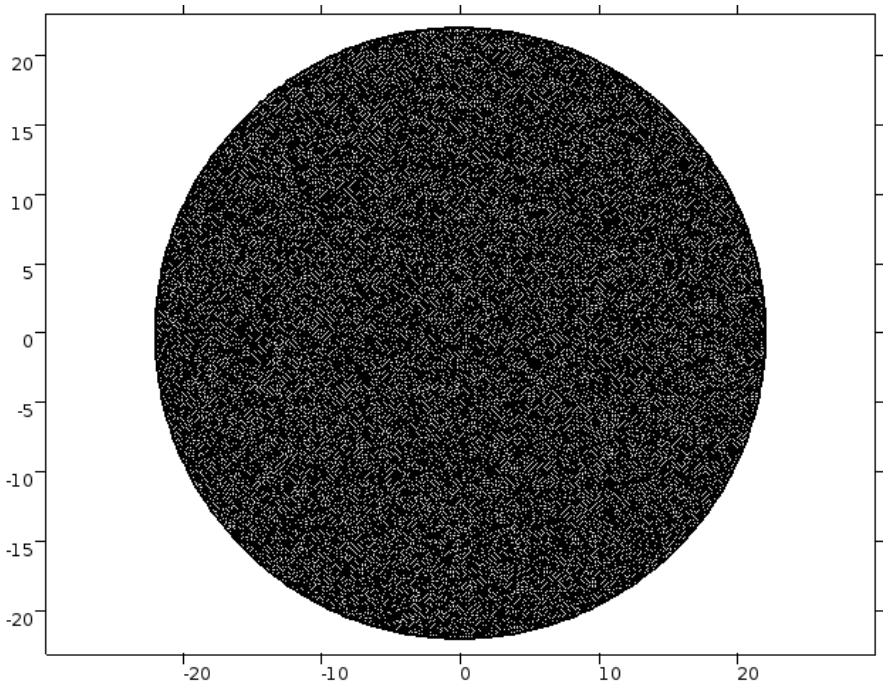

Figure 3.5: A snapshot from the custom dense mesh, containing 37.736 elements.

The mesh was built in a circular region with a dimensionless radius set to 22, as shown in Fig 3.5. A dimensionless radius of 22 is actually representing a tumor with a radius of 5,5 mm. A Delaunay triangulation was chosen for the mesh, containing a total of 37.736 triangular elements, of which 332 belong in the edges. The minimum element size was set at 0.0048 and the maximum one was set at 0.416. The maximum growth rate of each element was set to 1.08, and the curvature factor of elements was set to 0.25.

4. Results

4.1. Introductory Information

Two types of studies are going to be presented, one for bell distribution of CSCs, and one for noisy bell distribution of CSCs. For each type of distribution, a parametric study will be presented, and a basic study will be showcased as well, which represents a more rapidly growing tumor (in terms of tumor cells' growth rates).

For all studies, what is the main point of interest, is the growth rate of CSCs, prescribed as k_{15}. It represents how rapidly CSCs proliferate, and it is expressed as a fraction of the normal tumor cells' growth rate (in the same way CSCs' death rates are expressed as fractions of normal tumor cells' death rates). For these parameters, their dimensionless forms have the same relationship as their non-dimensionless, because their nondimensionalization factor is the same, namely $\frac{1}{k_{1,1}}$. E.g., if k_{15}^{*}= 2.4 * k_{12}^{*}, then k_{15} = 2.4 * k_{12}.

It is worth mentioning that, if not stated clearly, when time is referred in figures or in text, it is dimensionless time.

4.2. Bell CSCs Distribution Study

4.2.1. Basic Bell CSCs Distribution Study

It was decided to analyze the tumorous region of a cancer case, where k_{25} = 0.8 * k_{22}, and k_{15} = 1.2 * k_{12}. k_{12}^{*} parameter was set to 1.5, not 2, as in the Hubbard and Byrne 2012 publication [1].

The evolution of each phase's volumetric ratio will be shown at 6 dimensionless timestamps (0, 50, 100, 150, 200, 250) in each batch of simulation snapshots. The objective was to present data that are consistent with reality and the findings of Hubbard and Byrne's 2012 article [1]. By referring to consistency with reality, it is of

great importance to mention that CSCs need to be in a volumetric ratio ranging from 0,1% to 82,5%, as part of all phases. [25]. What is more, it is needed for tumor cells (normal and CSCs) to form the three-zone model that was referred in Chapter 3.1.1. (necrotic core, quiescent and proliferating zone), when the phenomenon has "matured", i.e., in the final dimensionless time. For CSCs, situated in niches, it is needed for them to have been relocated in hypoxic or proliferating regions of the tumor, where there will be enough nutrient for them to survive. Consequently, if there is no necrotic core formed, or if CSCs are inside the necrotic core, then the study must be reformed to different parameters, so it can fit scientific data.

The set of parameters that were selected, denoted a cancer type, where CSCs divide more rapidly than normal tumor cells, faster than in the previous studied cases. δ was set to 0.9.

The set of snapshots that will be displayed for the entire chapter, depicts phases inside the tumor, as well as the sum of θ_2 and θ_5, and the nutrient volumetric ratio inside the tumor. To make the findings similar, they are all scaled in the color range (0,1). Due to this, some volumetric ratios portrayals are scarcely discernible in comparison to the initial color ranges, indicating that the initial concentrations haven't changed much.

In the final dimensionless time, it is anticipated that:

- Healthy Cells will deplete in the areas where tumor cells are developing.
- Tumor Cells will form the three zones mentioned in the previous chapters.
- Blood Vessels phase will be denser in the quiescent and proliferating zone, and nearly unaltered in the region not influenced by the existence of tumor cells (normal or CSCs). There is also minimal to no blood vessels phase concentration in the necrotic core.
- Due to buildup of cellular waste, it is anticipated that the extracellular material will be most dense in the necrotic core.
- As the phenomenon develops, CSCs will leave the necrotic core in search of areas where they can survive in their niches.

All data are presented below:

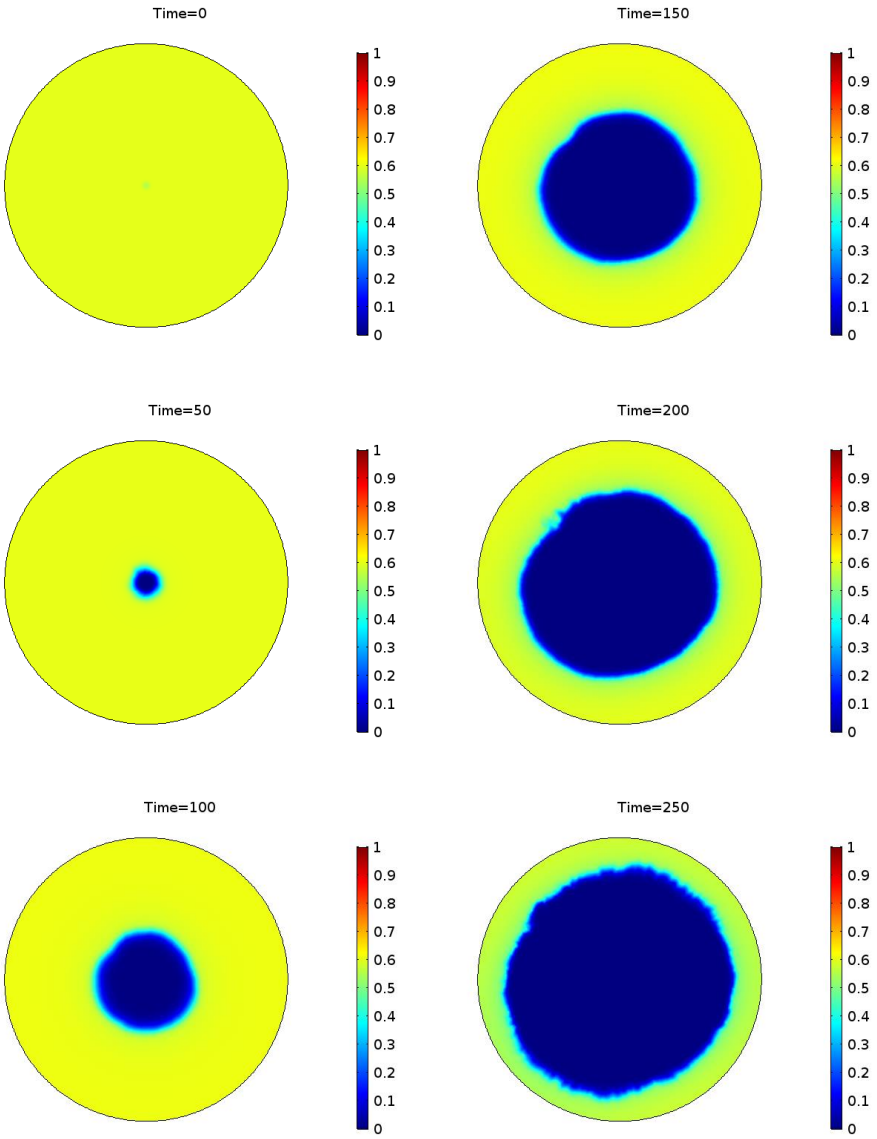

Figure 4.1: Healthy cells volumetric ratios for the basic Bell CSCs' initial distribution study

As expected, healthy cells shown in Fig.4.1, deplete in the center of the tumor, and parallelly, normal tumor cells rise in their concentrations, as shown in the snapshots below in Fig.4.2:

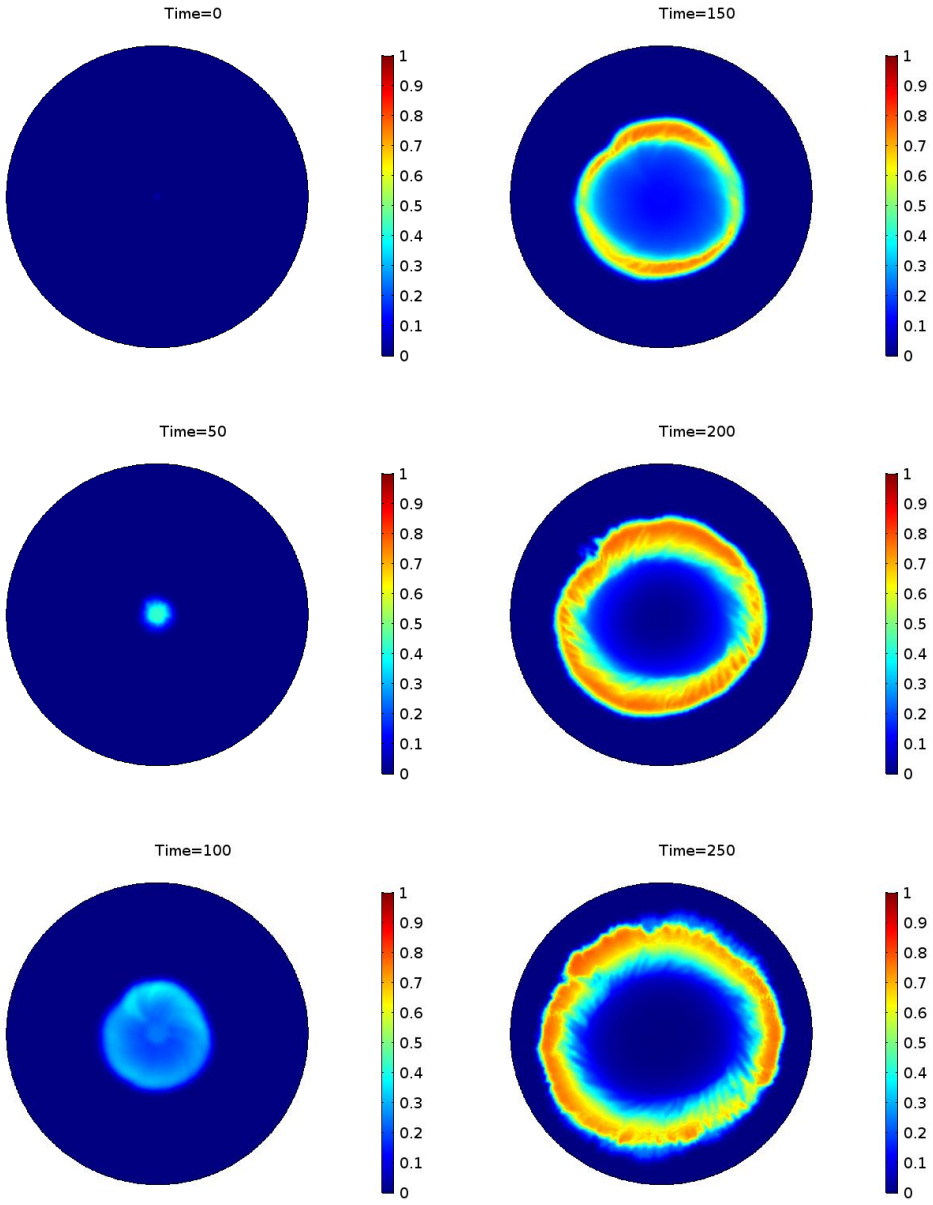

Figure 4.2: Normal tumor cells volume for the basic Bell CSCs' initial distribution study

In the final snapshot of Fig.4.2 (dimensionless time 250), the three-zone model is clearly depicted: A blue-hue circular region in center of the tumor is the necrotic core, while the whole volumetric ratios depicted with non-blue hues are the sum of the quiescent and the proliferating zone.

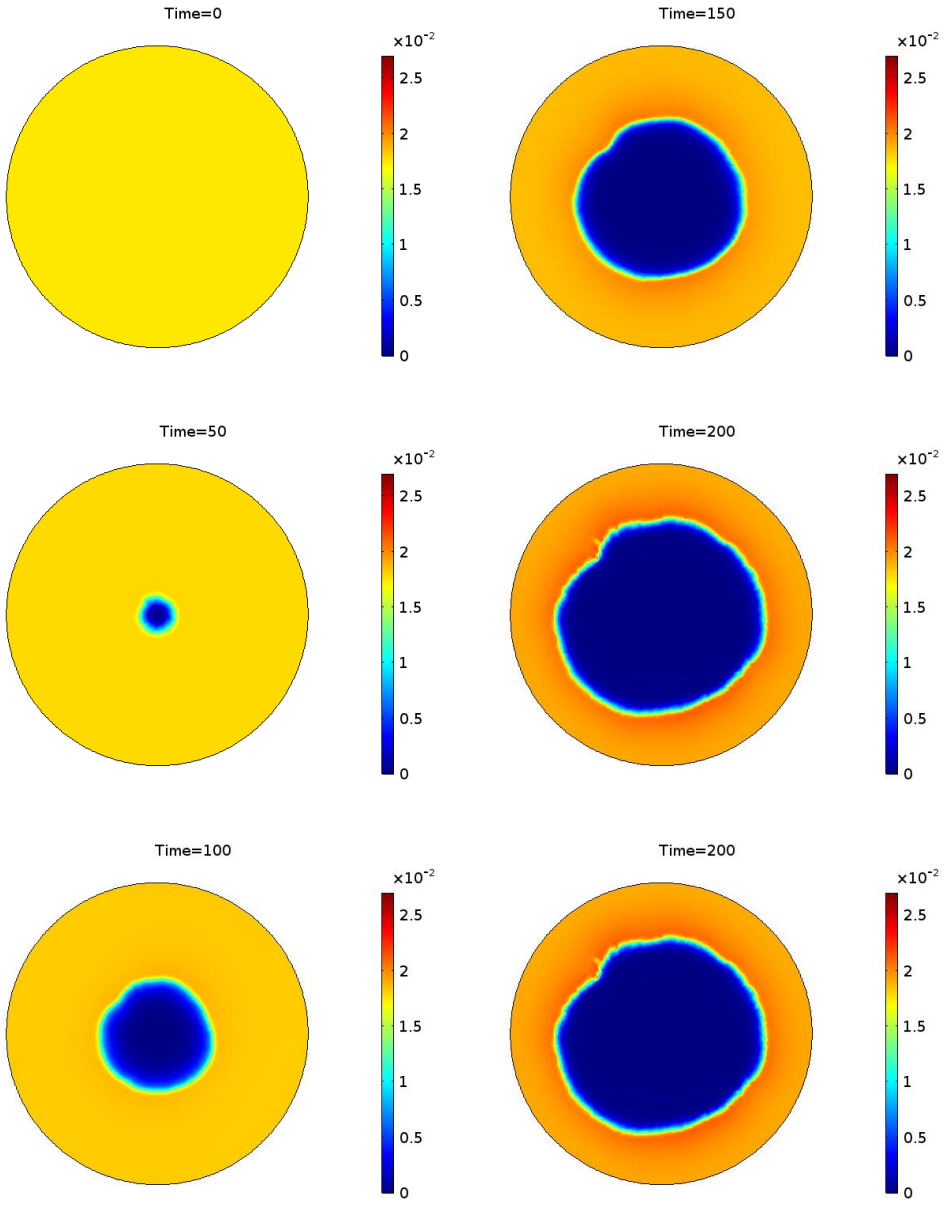

Figure 4.3: Blood Vessels volumetric ratio fractions for the basic Bell CSCs' initial distribution study

According to the Hubbard and Byrne 2012 publication [1], the blood vessels phase is present in relatively low amounts, when compared to other phases' volumetric ratios. The blood vessels phase in that area decreases as the necrotic center expands, as seen in the snapshots of Fig.4.3.

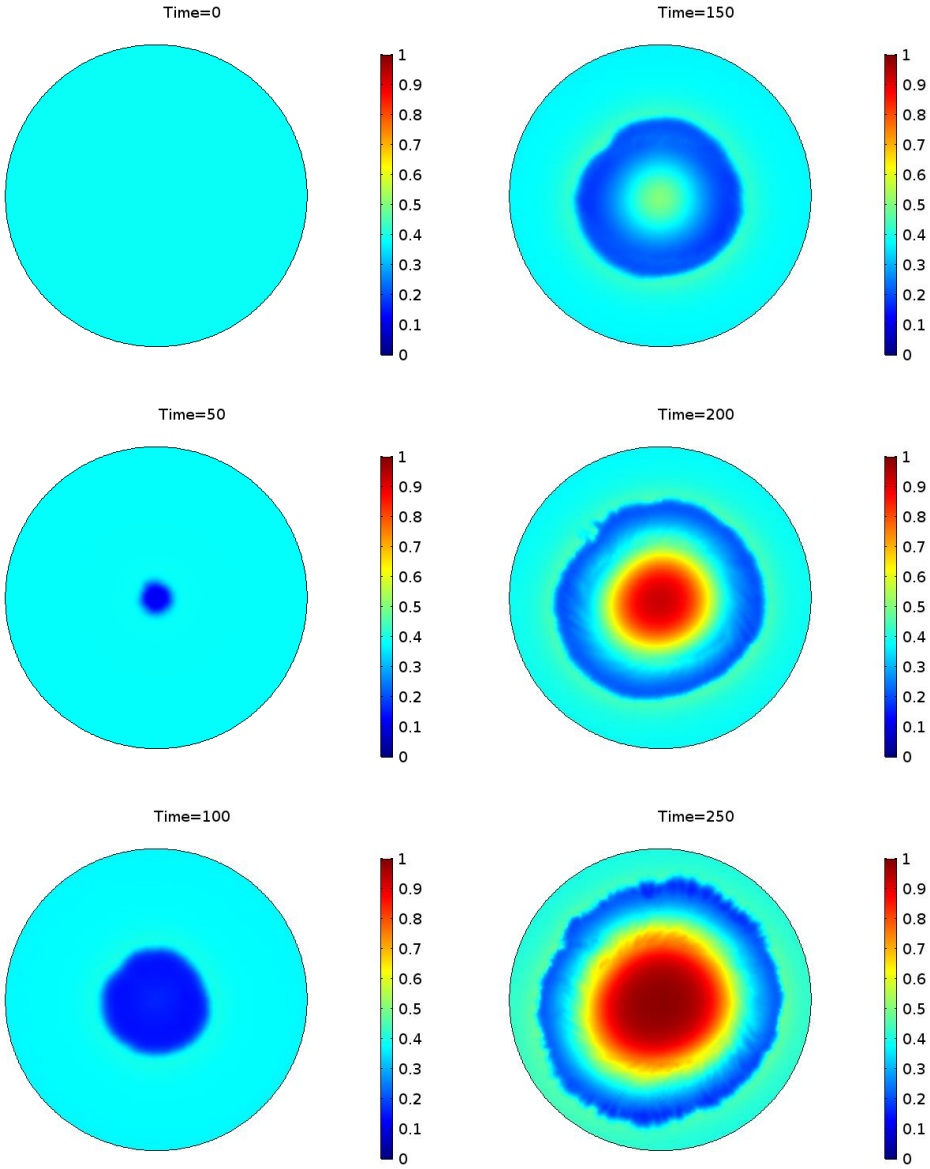

Figure 4.4: Extracellular Material (ECM) volumetric ratio evolution for the basic Bell CSCs' initial distribution study

The development of the ECM phase is the opposite of how the tumor cells develop. While the ECM phase steadily declines near the end of the proliferative zone, as shown in the snapshots' dimensionless time evolution in Fig. 4.4, the necrotic core is abundant in ECM (particularly dead cells, which are also ECM). Due to the tumor cells' lack of influence outside if this area, the remainder of the ECM phase maintains a nearly unaltered concentration there.

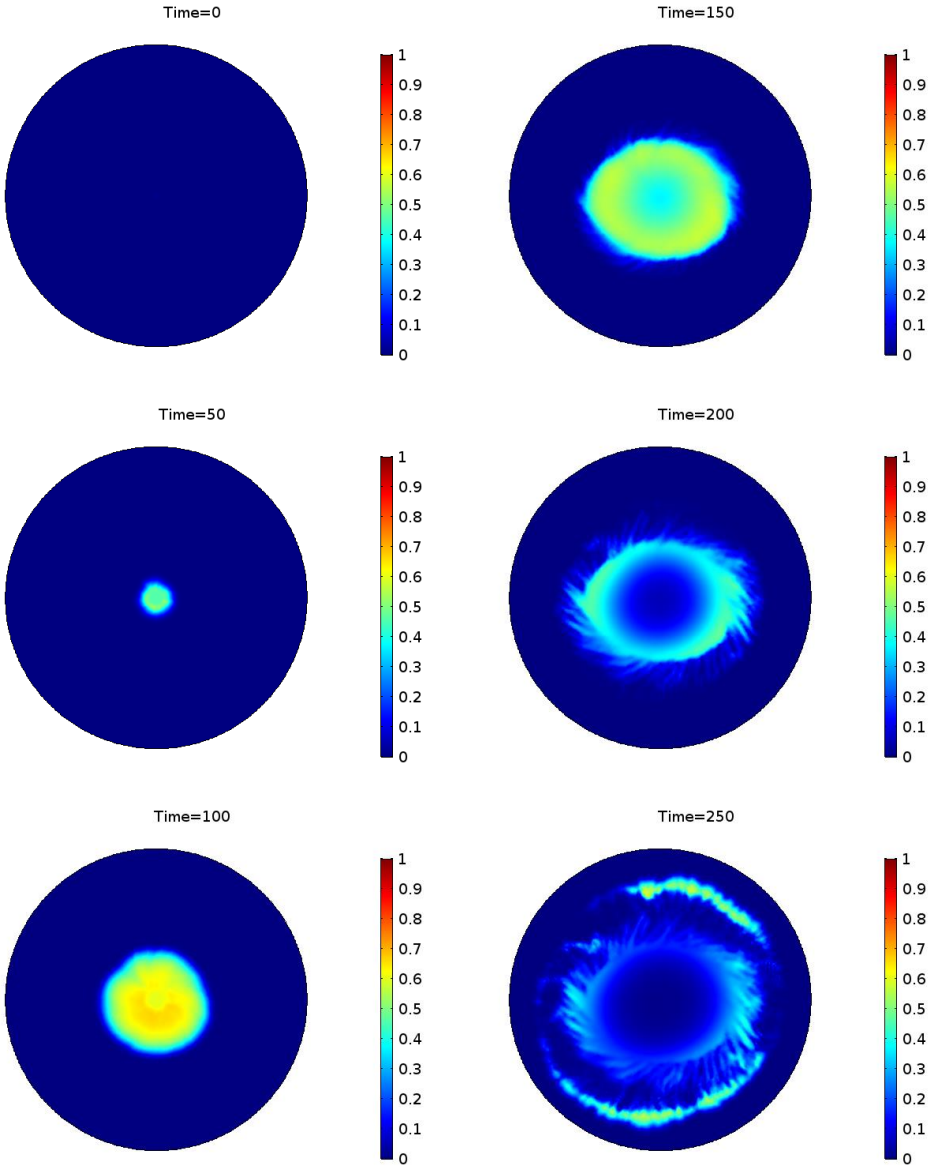

Figure 4.5: CSCs volumetric ratio fractions for the basic Bell CSCs' initial distribution study

As anticipated, CSCs in Fig.4.5. are shown to slowly increase in concentration, before leaving the necrotic core. The normal tumor cells' snapshots (Fig. 4.2), as well as the snapshots in Fig. 4.5., revealed that the endpoints of the proliferating zone, where there is abundant nutrient, had the highest concentrations of CSCs.

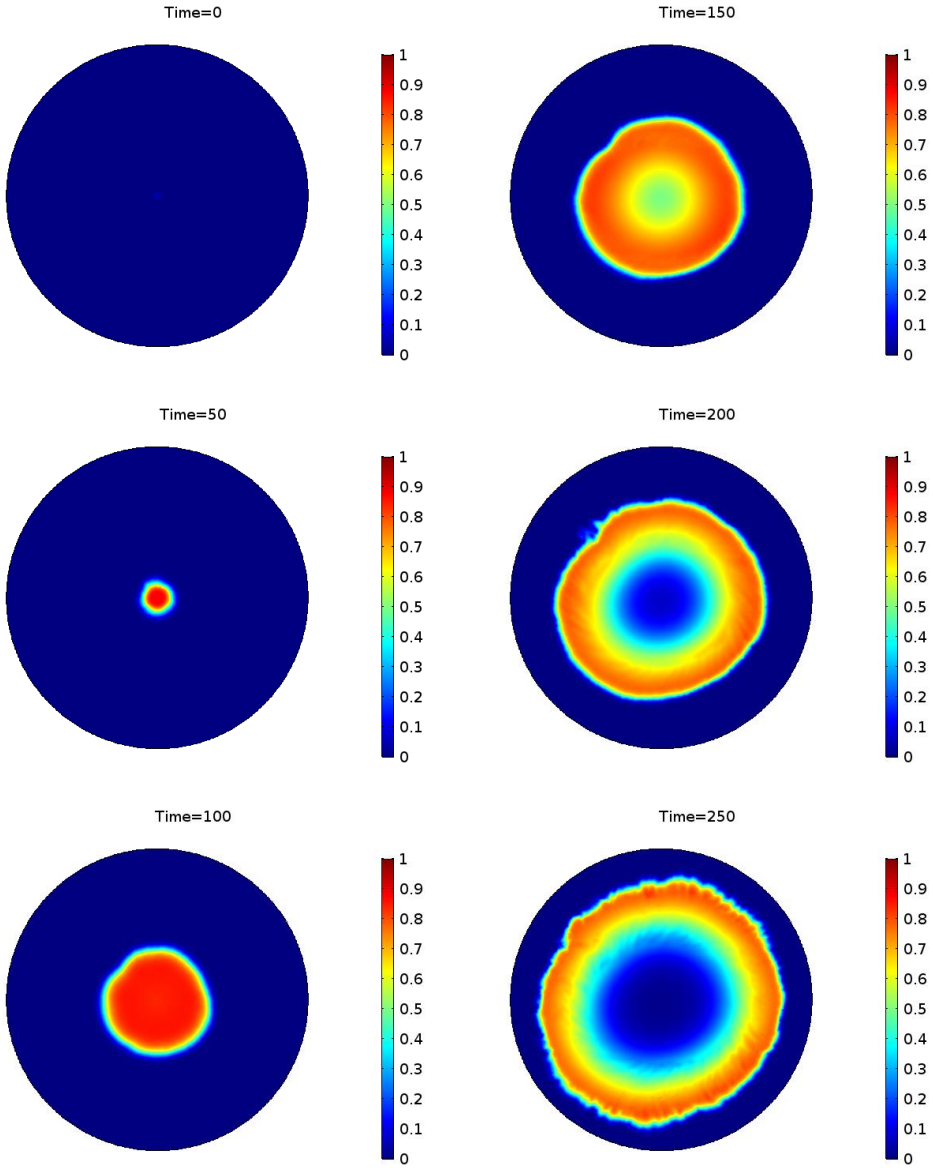

Figure 4.6: CSCs and normal tumor cells phases volumetric ratios for the basic Bell CSCs' initial distribution study

The whole three-zones model, which is consistent with what is anticipated, is made up of both CSCs and normal tumor cells combined, as shown in Fig.4.6. The absence of tumor cells, either normal or CSCs in the necrotic core indicates that the simulated phenomenon has "matured" enough in the final dimensionless time 250.

The snapshots of nutrient volumetric ratios are the last. According to the projected evolution pattern of the blood vessels phase, it will be scarce inside the necrotic center and dense outside of it. And it happens that way, as shown in Fig.4.7.

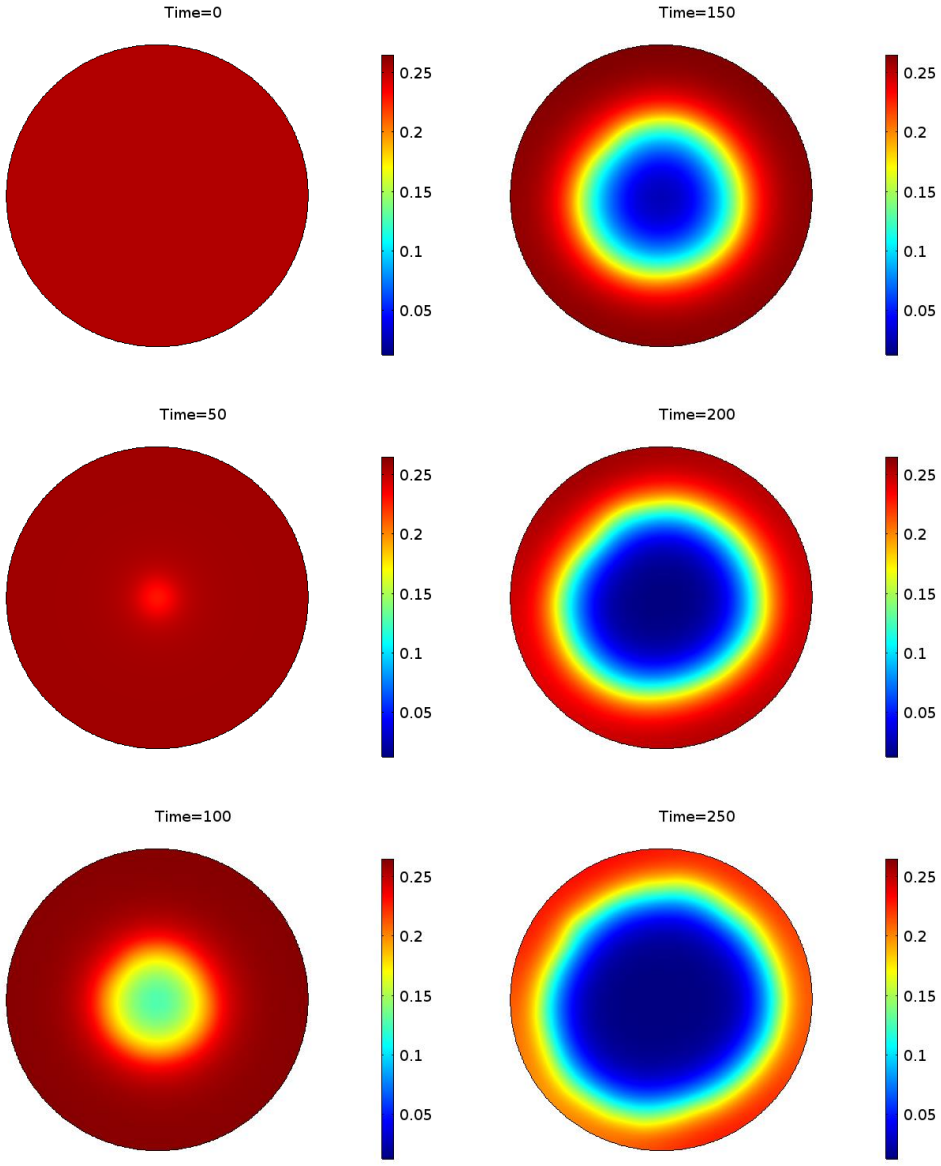

Figure 4.7: Oxygen volumetric ratios for the basic bell CSCs' initial distribution study

The evolution of all phases, as well as of the nutrient, can be depicted in the volumetric ratios diagram, in Fig.4.8, as dimensionless time evolves:

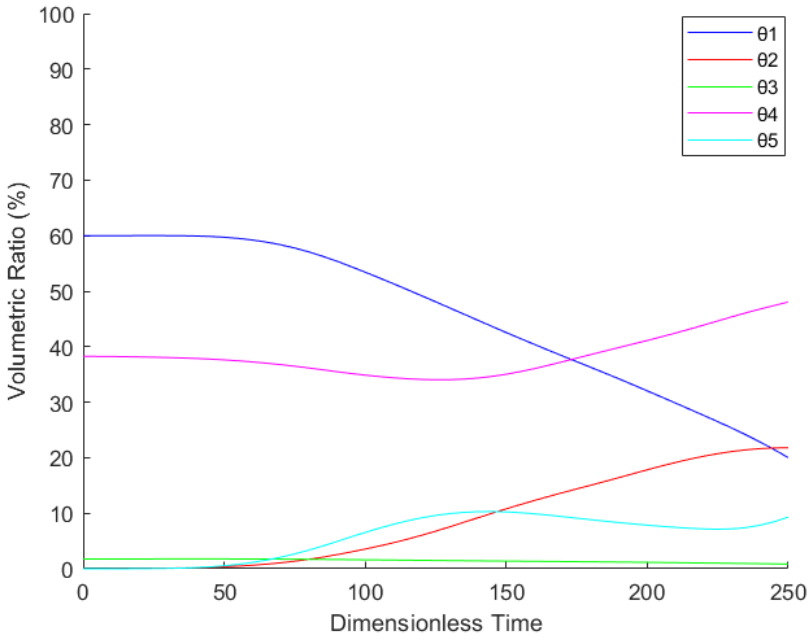

Figure 4.8: All phases' volumetric ratios, as simulation dimensionless time evolves, for the basic Bell CSCs' initial distribution study

The evolution of dimensionless time is seen in all 5 phases. Since Θ_5 (CSCs) have a lower volumetric ratio than other phases, separate diagrams have been created to show both the CSCs' volumetric ratios and how they compare to the volumetric ratios of normal tumor cells.

As shown in the figure, normal tumor cells grow as dimensionless time rises, whereas healthy cells decline monotonically after a fixed amount of dimensionless time. Both are reasonable conclusions given that normal tumor cells exhibit higher dimensionless rates of growth than healthy cells, and nower dimensionless rates of death than healthy cells. Specifically:

$k_{1,2} > k_{1,1}$, since $k^*_{1,2} = \frac{k_{1,2}}{k_{1,1}} = 1.5$, set for the basic model (while for the parametric study it is set to 2).

$k_{2,1} > k_{2,2}$, since $k^*_{2,1} = \frac{k_{2,1}}{k_{1,1}} = 0.15$ and $k^*_{2,2} = \frac{k_{2,2}}{k_{1,1}} = 0.075$, both set for all studies in this thesis. Consequently, $\frac{k_{2,1}}{k_{2,2}} = 2$.

The blood vessels achieve their end volumetric ratio value at 1,27%, which is less than half of the initial volumetric ratio (2,66%), and require a separate diagram as a result of their low volumetric ratio. This is in accordance with the the evolution of blood vessels phase volumetric ratio described in the Hubbard and Byrne 2012 study [1].

As for the ECM phase, it makes sense that the volumetric ratio will peak at the last dimensionless time. As the phenomenon progresses, the high surface percentage occupied by the necrotic core, dictates that a high percentage of the materials are dead cells, which belongs in the θ_4 phase.

To demonstrate the existence of the three zones model in numerical form as well, it is now necessary to observe some numerical data. The figures that follow show how the volumetric ratio in the tumorous zone changes as the radius grows. While some figures will be in the traditional time range (0, 50, 100, 150, 200, 250), the majority will be in the final dimensionless time.

The figures illustrating the formation of the necrotic core, in which there is few or no blood vessels phase volumetric ratio, come first. Thus, the vascularity increases where the necrotic core terminates.

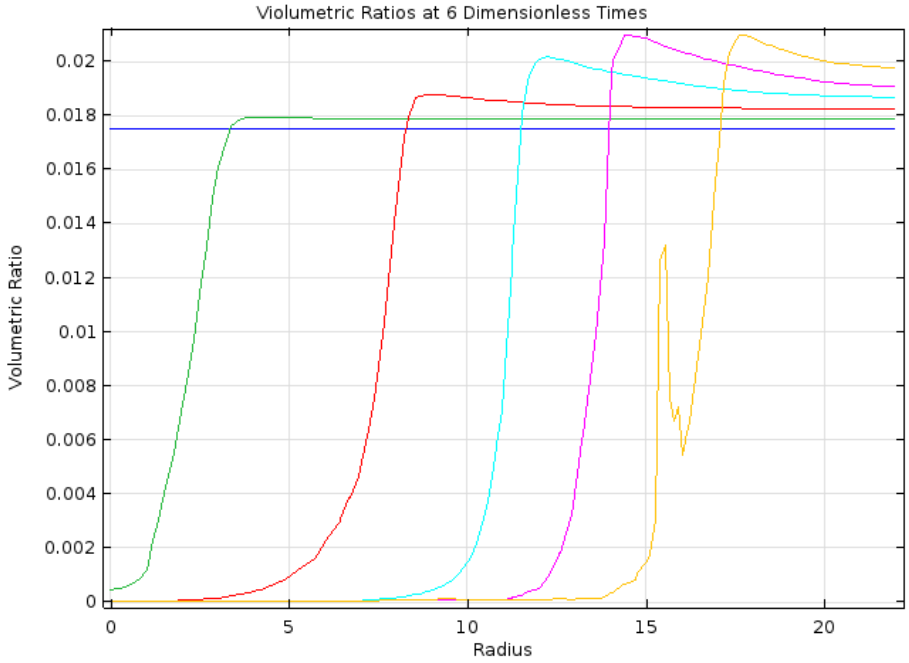

Figure 4.9: Blood vessels phase volumetric ratios as radius increases for the basic Bell CSCs' initial distribution study.

Fig.4.9 displays the volumetric ratio of blood vessels during the course of the studied times (0, 50, 100, 150, 200, 250) from blue to orange (in this radius increasing order), with increasing maximum value from left to right. When the nutrition levels are insufficient for tumor cells to survive, dead cells (which are part of the ECM phase) condense in this area, creating the necrotic core. Furthermore, there is no vascularity in the necrotic core. For dimensionless time 0, there is an initial blood vessels volumetric ratio that, as time increases, begins to decrease in the lower spectrum of radii. A little increase in θ_3 volumetric ratio starts from radius for dimensionless period 250, and then, roughly, a large increase starts from radius 14. Fig.4.10, which essentially is an enlarged diagram of the blood vessels phase volumetric ration in dimensionless time 250, clearly illustrates that.

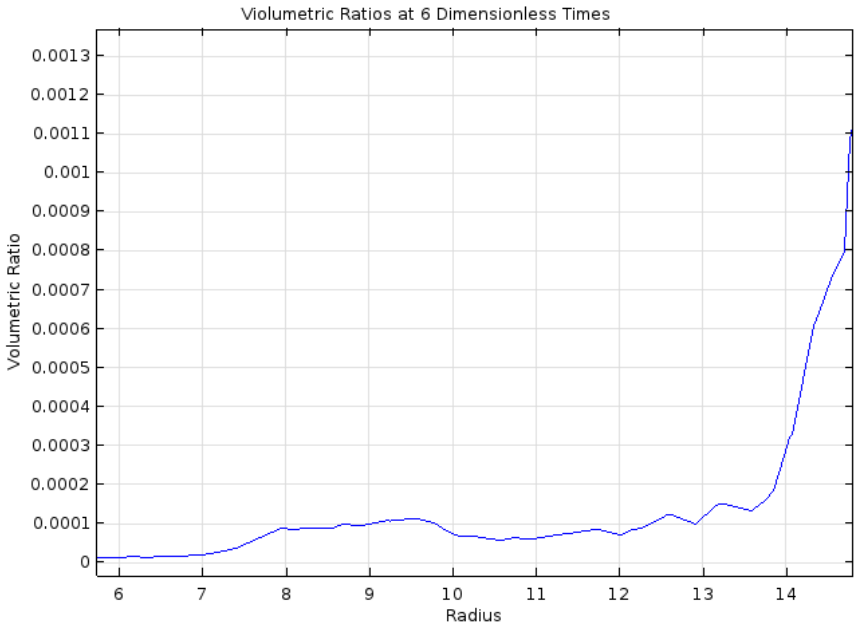

Figure 4.10: Enlarged blood vessels phase volumetric ratios diagram as radius increases, for the basic Bell CSCs' initial distribution study.

This indicates that the necrotic core begins at zero radius and then fades outward starting at radius 7 and continuing until radius 14, which is clearly visible in the volumetric ratio of total tumor cells, as a function of radius, in the final dimensionless time:

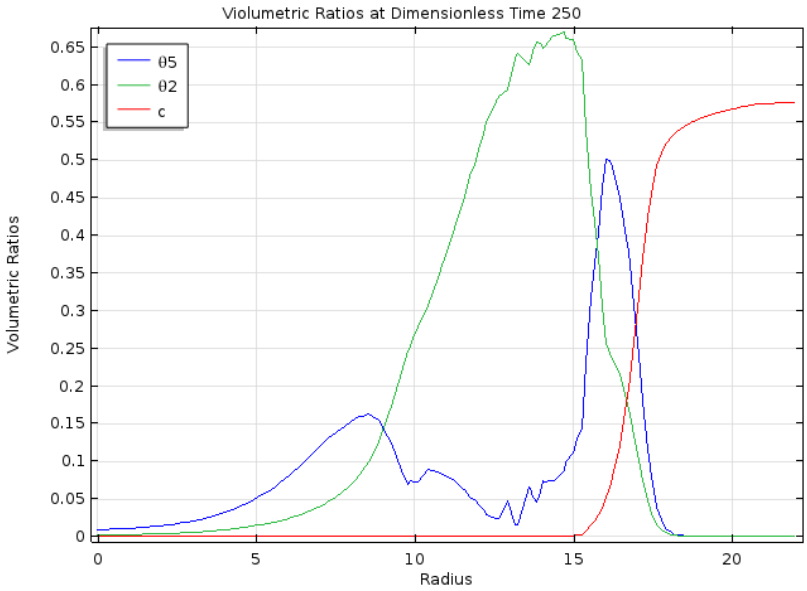

Figure 4.11: Normal tumor cells, CSCs and nutrient volumetric ratios as radius increases, for the basic Bell CSCs' initial distribution study.

More clarity regarding tumor cell densities in the three zones will be provided in Fig. 4.11. As can be seen, the volumetric ratio of normal tumor cells increases roughly from radius 7 to radius 14, which indicates that the quiescent zone eventually takes over the region that the necrotic core originally occupied. The proliferating zone begins after radius 14, where there are two graph peaks.

4.2.2. A Parametric Study on Bell CSCs Distribution

A Bell CSCs initial distribution parametric study was carried out using the same mesh, the same radius for the circular region analyzed, the same initial conditions, and the same parameters as indicated in chapter 3. However, there are two significant variations, namely the normal tumor cells' growth rates, and the growth and death parameters of CSCs. k_{12}^* was set at 2 (the value of the Hubbard and Byrne paper [1]), and not at 1.5. k_{15}^* was the subject of the parametric analysis, as its value fluctuated, and 5 simulations were run in total, for (0.75, 0.875, 1.0, 1.125, 1.25) * k_{12}^*. k_{25}^* was stably set at 0.8 * k_{22}^*. Of greater importance was to showcase how CSCs proliferate and relocate inside the studied region. Thus, for this and for the next parametric study, simulation snapshots (Fig. 4.14 and Fig. 4.27) were given only for the CSCs phase.

Although the dimensionless time was set to be studied from 0 to 250, (time step was set at 5), after dimensionless time 230, there was at least one simulation in this or the next parametric study that the cell phases reached the boundaries of the simulated region, which is unacceptable for simulation validity reasons. As a result, it was deemed that setting the computed simulation's final time limit at 230 was the best course of action.

Not all simulations agreed with the scientific data, either as a result of very low CSCs volumetric ratios (lower than 0,1% [25]), or because CSCs were present in the necrotic core, despite the necrotic core's lack of oxygen supply.

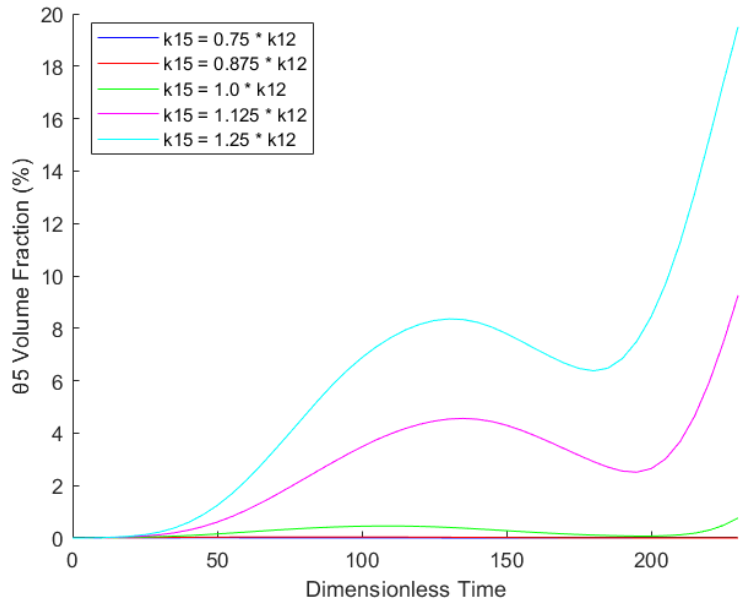

Figure 4.12: Cancer stem cells Volumetric ratios for different k_{15} values, and k_{25} = 0.8 * k_{22} (parametric study for Bell CSCs' initial distribution)

As shown in Fig. 4.12, CSCs' volumetric ratio follows the same pattern, as the one in the basic modeling procedure. Nevertheless, for. k_{15} value lower than 1.0 of k_{12}, the volumetric ratio of CSCs is barely visible, thus an enlarging figure (Fig.4.13) was made.

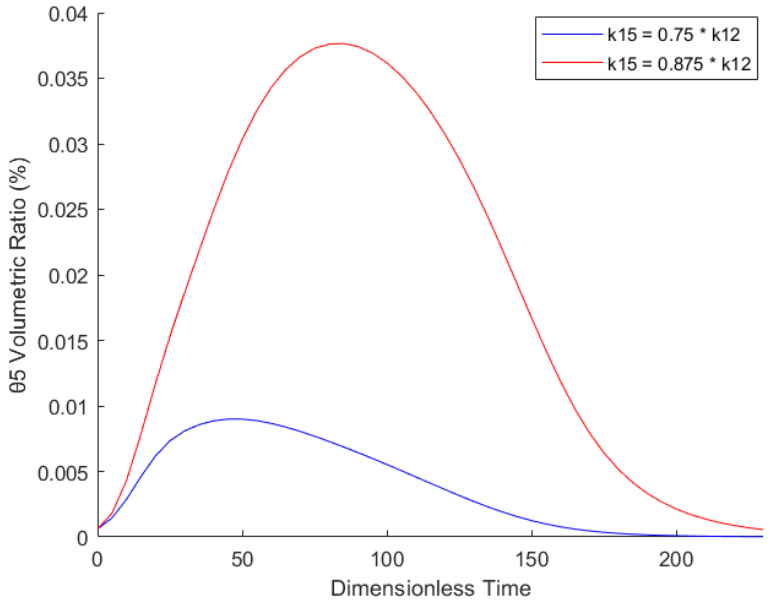

Figure 4.13: An enlarged figure of Cancer stem cells Volumetric ratios for different k_{15} values, and k_{25} = 0.8 * k_{22} (parametric study for Bell CSCs' initial distribution)

The greatest volumetric ratio of CSCs, as demonstrated above, is less than 0,1% for k_{15} values lower than 0.875 of k_{12}, which does not reflect scientific reality for minimum CSCs existence inside a tumor. The final CSCs volumetric ratios for each study were as follows:

- For $k_{15} = 0.75 * k_{12}$: 1,93 * 10^{-5} %
- For $k_{15} = 0.875 * k_{12}$: 5,57 * 10^{-4} %
- For $k_{15} = 1.0 * k_{12}$: 0,76%
- For $k_{15} = 1.125 * k_{12}$: 9,25%
- For $k_{15} = 1.25 * k_{12}$: 19,50%

Given that CSCs must have a volumetric ratio of at least 0,1%, k_{15} must have a value greater than 0.875 of k_{12}, if k_{25} has a value greater than 80% of k_{22}. As seen in the results below, the results are satisfactory for k_{15} equal to k_{12} or greater, because CSCs exit the necrotic core in the end simulated dimensionless time. For k_{15} values equal to 0.75 and 0.875 of k_{12}, CSCs are not even visible, as shown in Fig. 4.14:

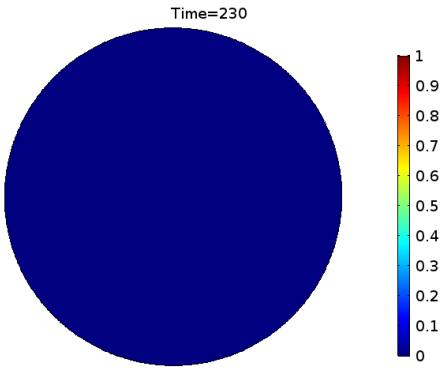

$k_{15} = 0.75 * k_{12}$

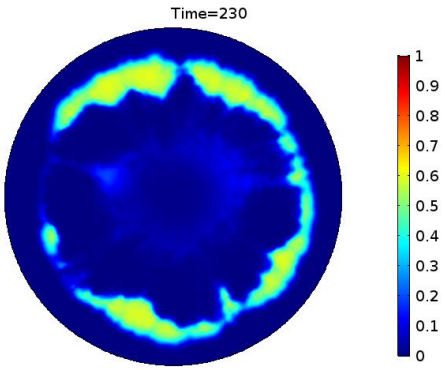

$k_{15} = 1.125 * k_{12}$

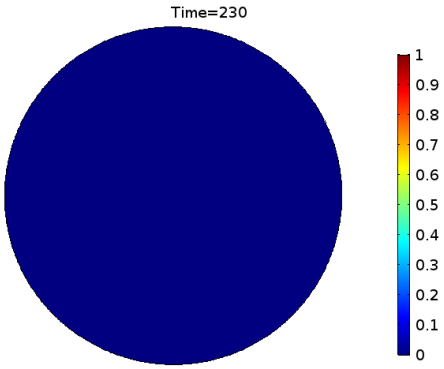

$k_{15} = 0.875 * k_{12}$

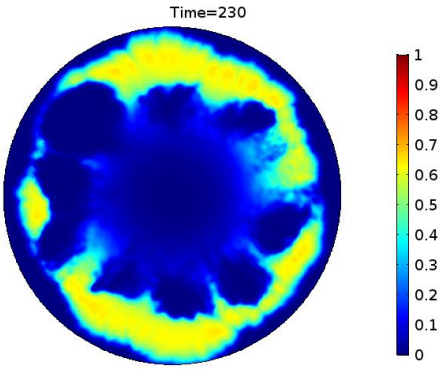

$k_{15} = 1.25 * k_{12}$

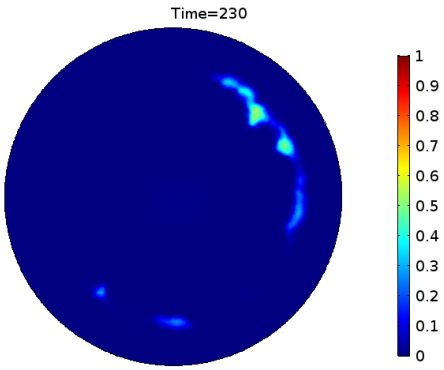

$k_{15} = 1.0 * k_{12}$

Figure 4.14: Snapshots of CSCs volumetric ratios in the final showcased time (parametric study for Bell CSCs' initial distribution)

4.3. Noisy Bell CSCs Distribution Study

4.3.1. Basic Noisy Bell CSCs Distribution Study

A similar basic study as before was carried out, except time CSCs were in noisy bell initial distribution. All the other parameters are the same as in the Chapter 4.2.1. (k_{12}^{*}=1.5 as well), and the majority of snapshots are quite like the ones in previous study, but the minor differences will be explained. Below are shown the snapshots for θ_1, θ_3, θ_4, θ_5 and oxygen, respectively (Fig. 4.15, Fig. 4.16, Fig. 4.17, Fig. 4.18):

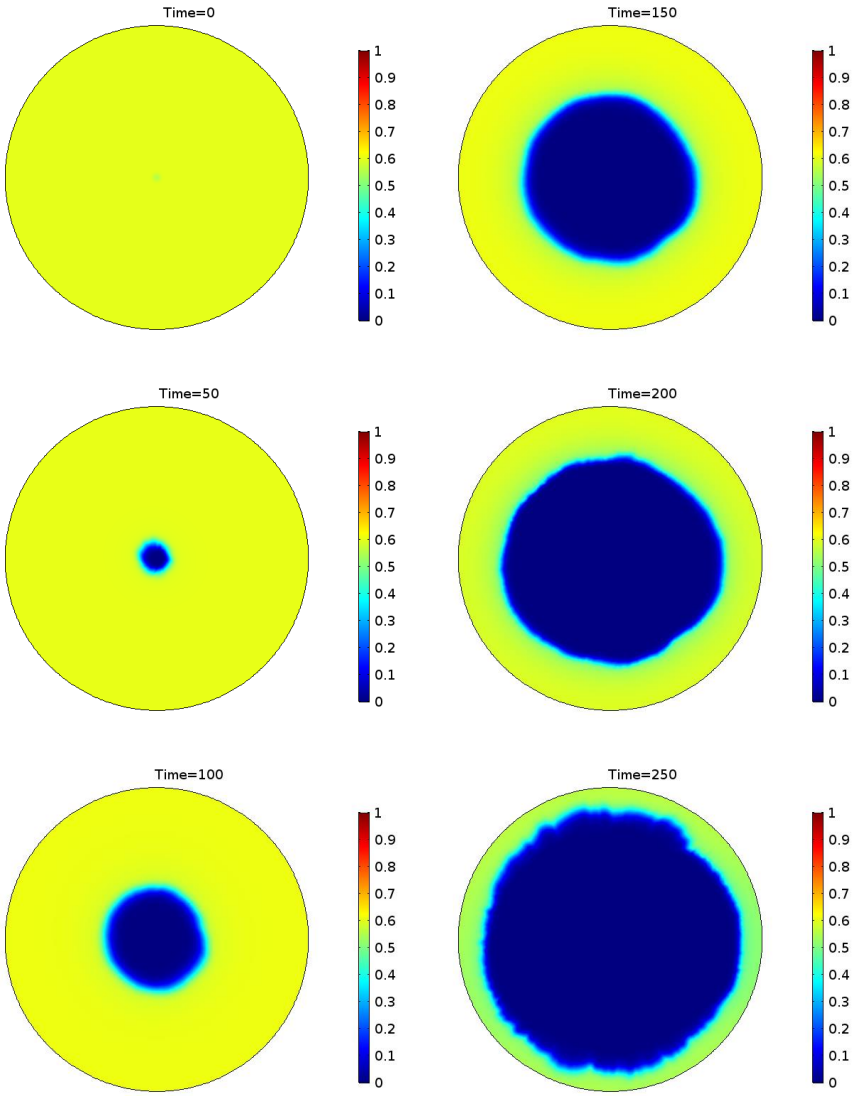

Figure 4.15: Healthy cells volumetric ratio fractions for the basic Noisy Bell CSCs' initial distribution study

In comparison with Fig. 4.16, healthy cells in Fig. 4.1 are more widely distributed in the ends of the studied area. In the next chapter, the comparison of end volumetric ratios (in dimensionless time 250 for both basic studies (Chapters 4.2, 4.4.), will showcase the difference in their volumetric ratio.

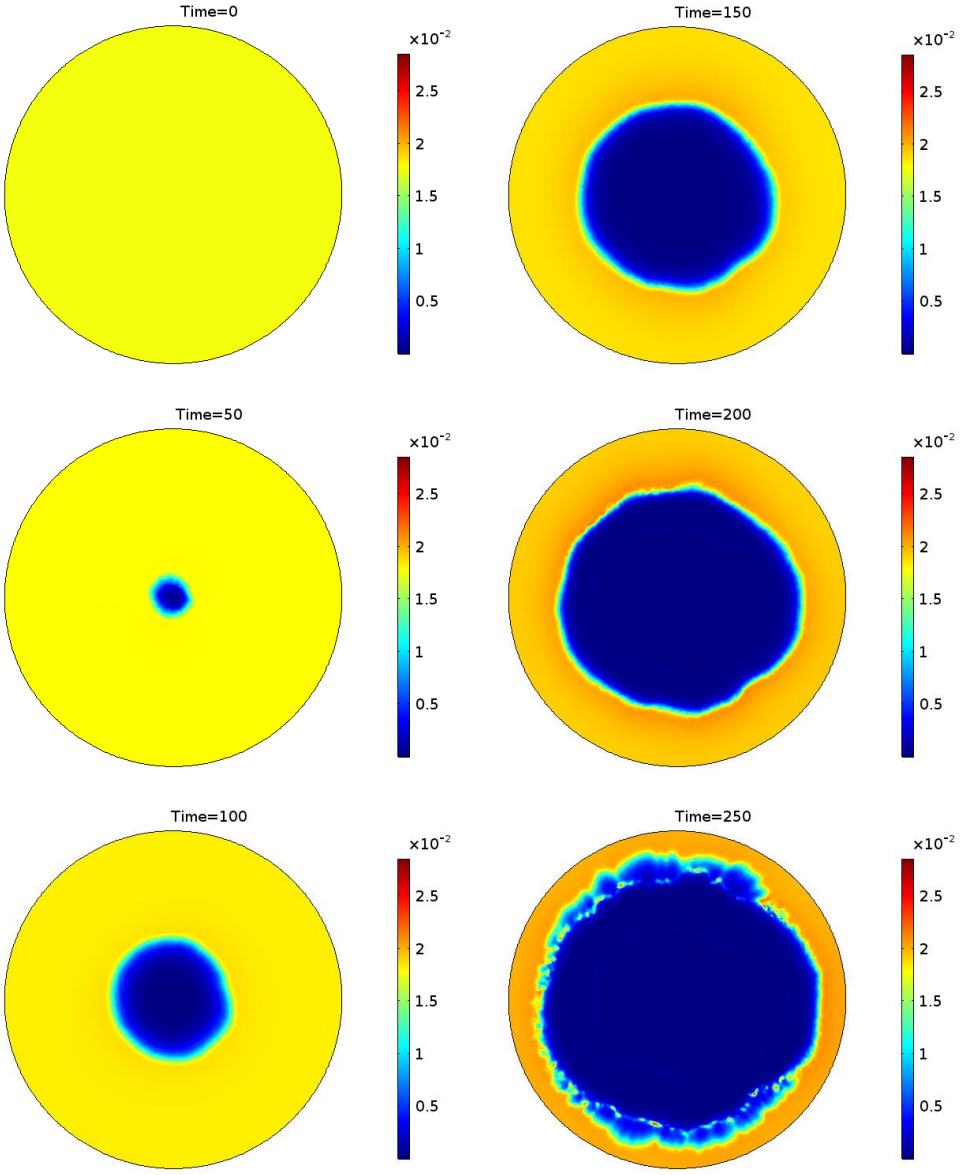

Figure 4.16: Blood vessels volumetric ratio fractions for the basic Noisy Bell CSCs' initial distribution study

Fig. 4.16 shows a more widely distributed lack of vascularity in the studied region center, compared to Fig.4.3.

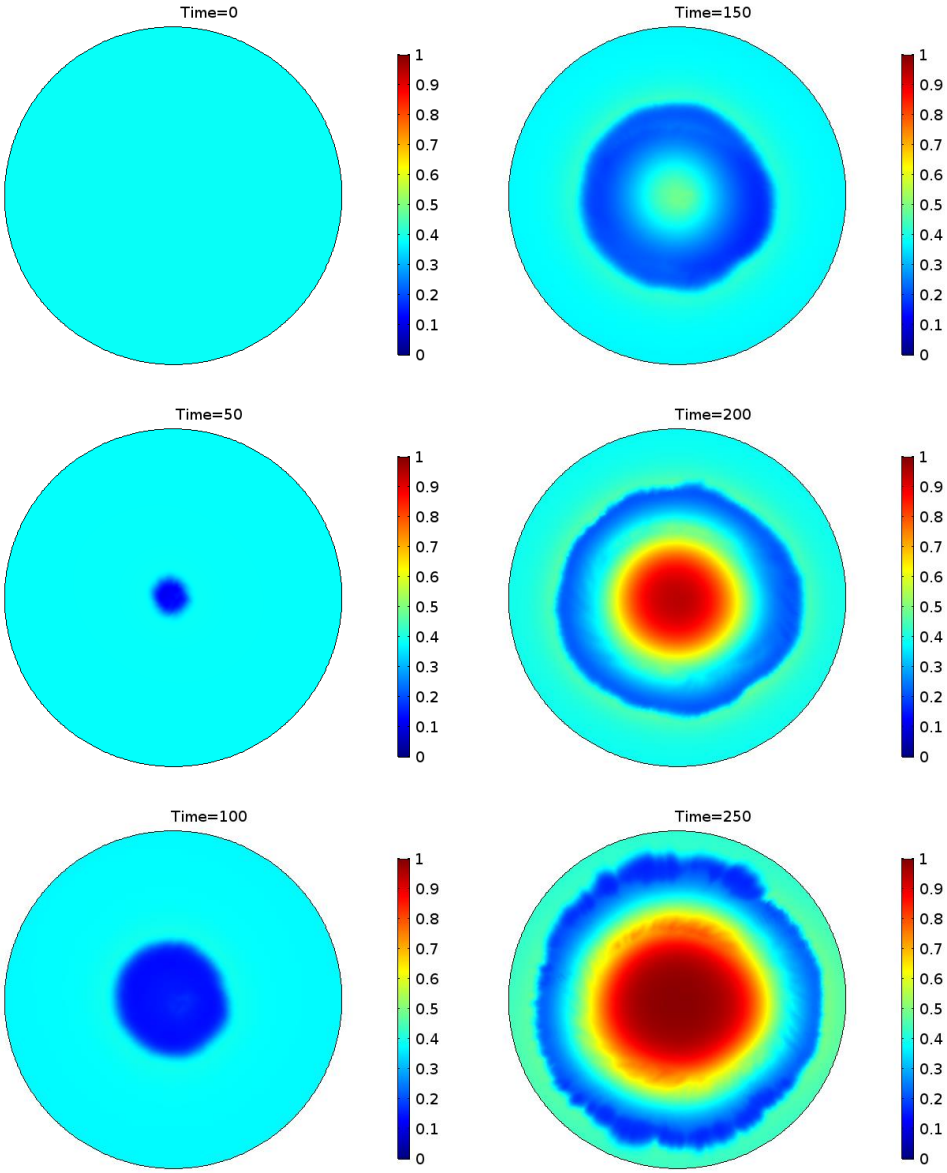

Figure 4.17: Extracellular Material (ECM) volumetric ratio fractions for the basic Noisy Bell CSCs' initial distribution study

ECM phase in final dimensionless time, in Fig.4.17, is again richer in concentration, than in the final dimensionless time in Fig.4.4.

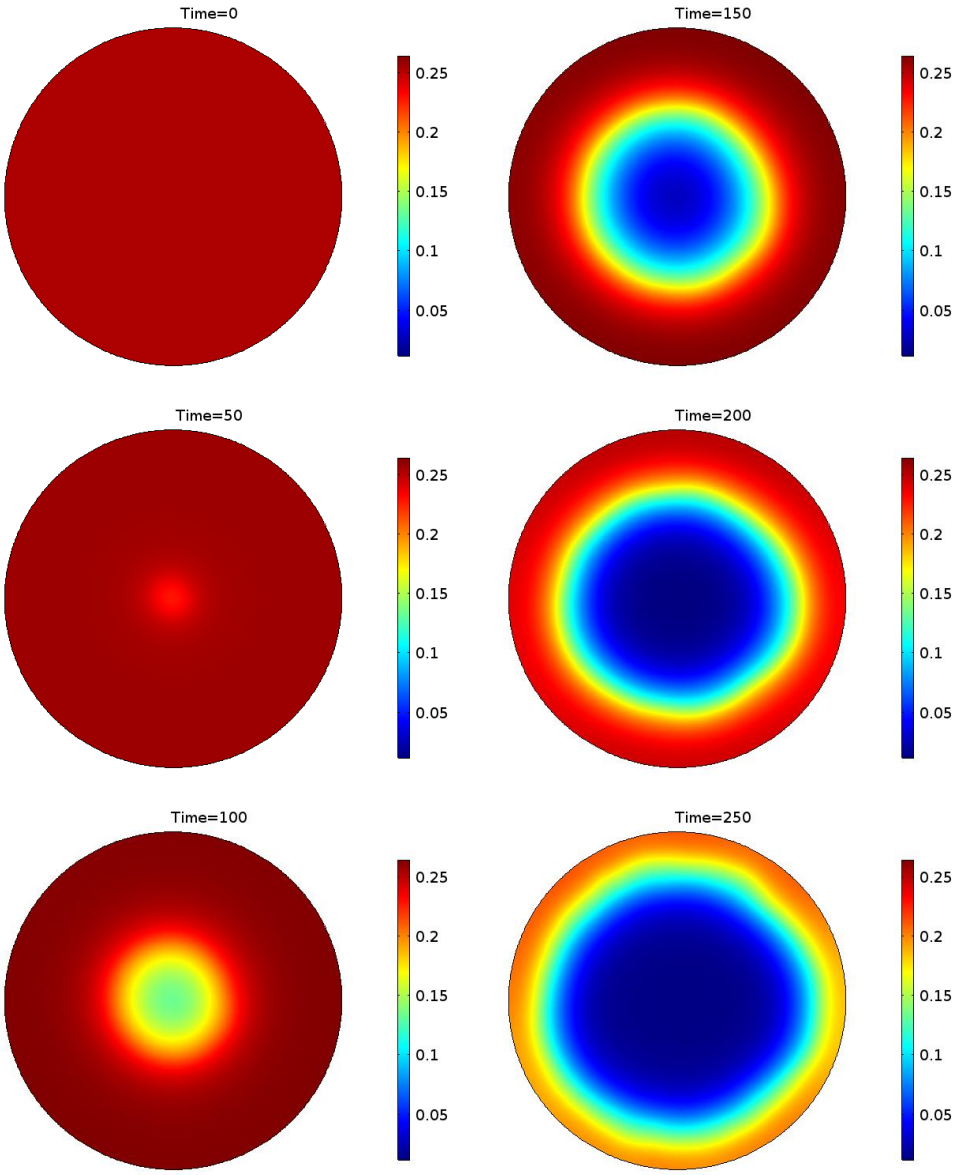

Figure 4.18: Oxygen volumetric ratios for the basic Noisy Bell CSCs' initial distribution study

Again, the set of snapshots in Fig.4.18 shows the same tendencies pattern as those in Fig. 4.15 and Fig. 4.16. There is a wider distributed lack of oxygen in the center of the studied region, compared to that of Fig.4.7.

The following figure (Fig.4.19) will showcase the distribution of normal tumor cells, and in combination with Fig.4.20 (CSCs distribution inside the studied region), will set up the boundaries for the three-zone model.

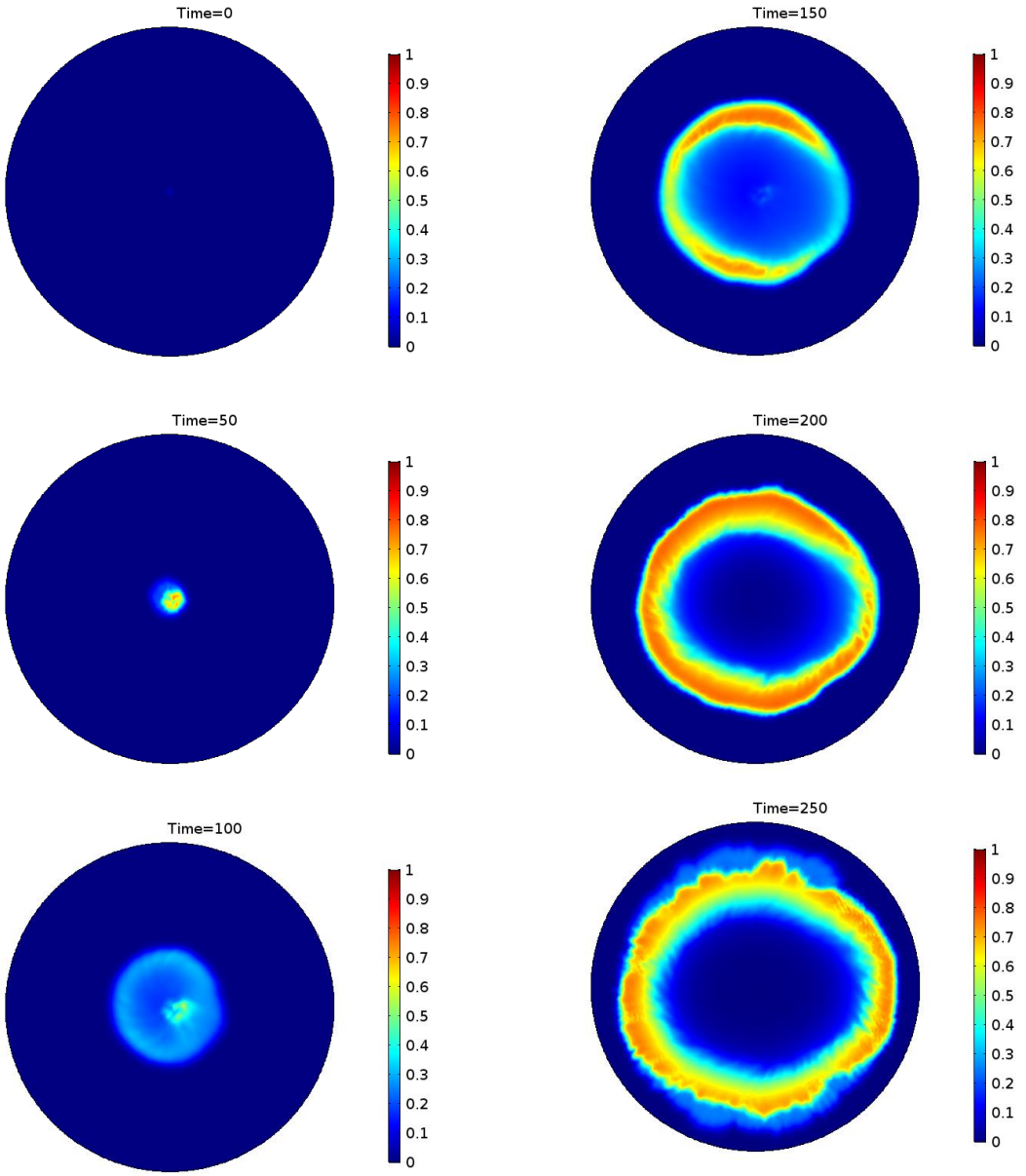

Figure 4.19: Normal tumor cells volumetric ratio fractions for the basic Noisy Bell CSCs' initial distribution study

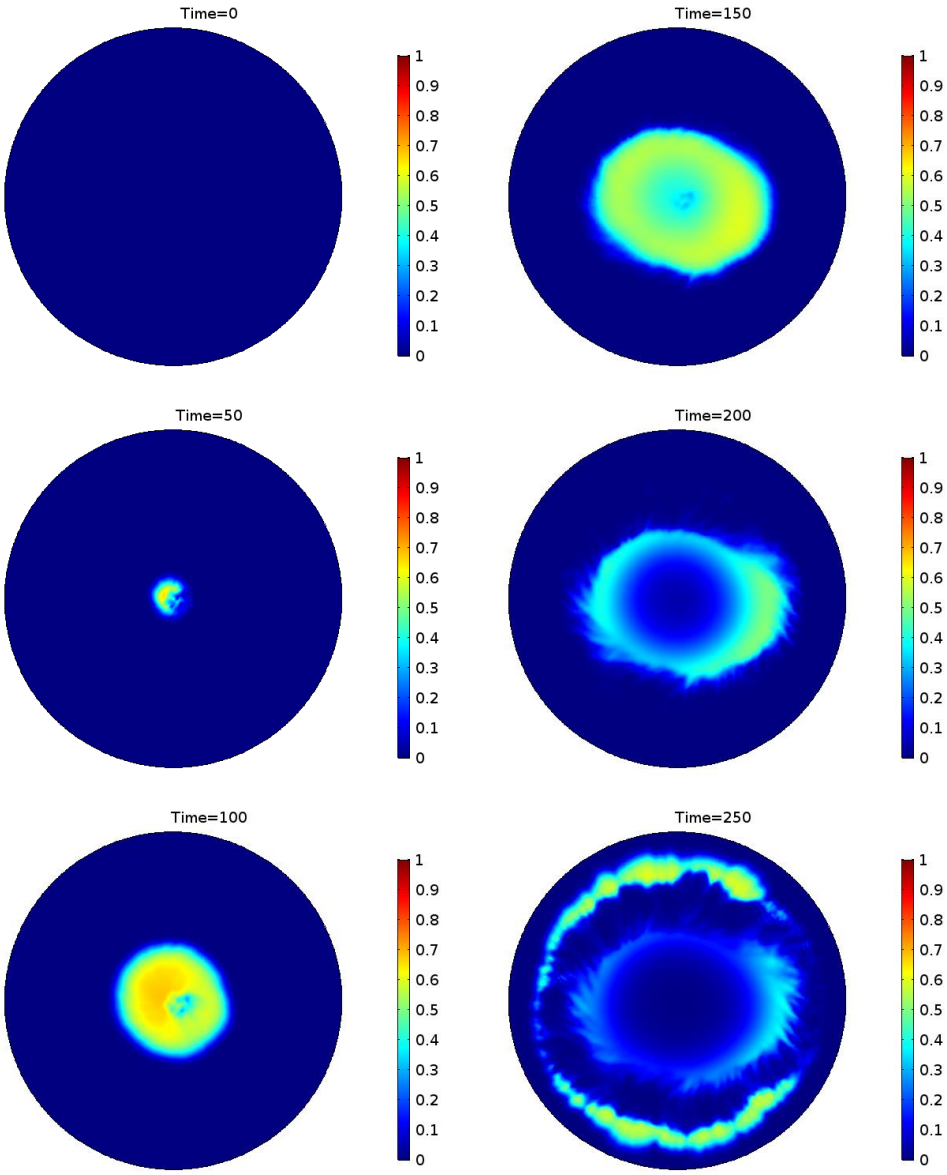

Figure 4.20: Cancer stem cells (CSCs) volumetric ratio fractions for the basic Noisy Bell CSCs' initial distribution study

As demonstrated above (Fig.4.20), CSCs are slightly higher concentrated than in the bell study, which will be shown in the Conclusions chapter as well. The last figure (Fig. 4.21) represents the total volume of normal tumor cells and CSCs over the 6 dimensionless times.

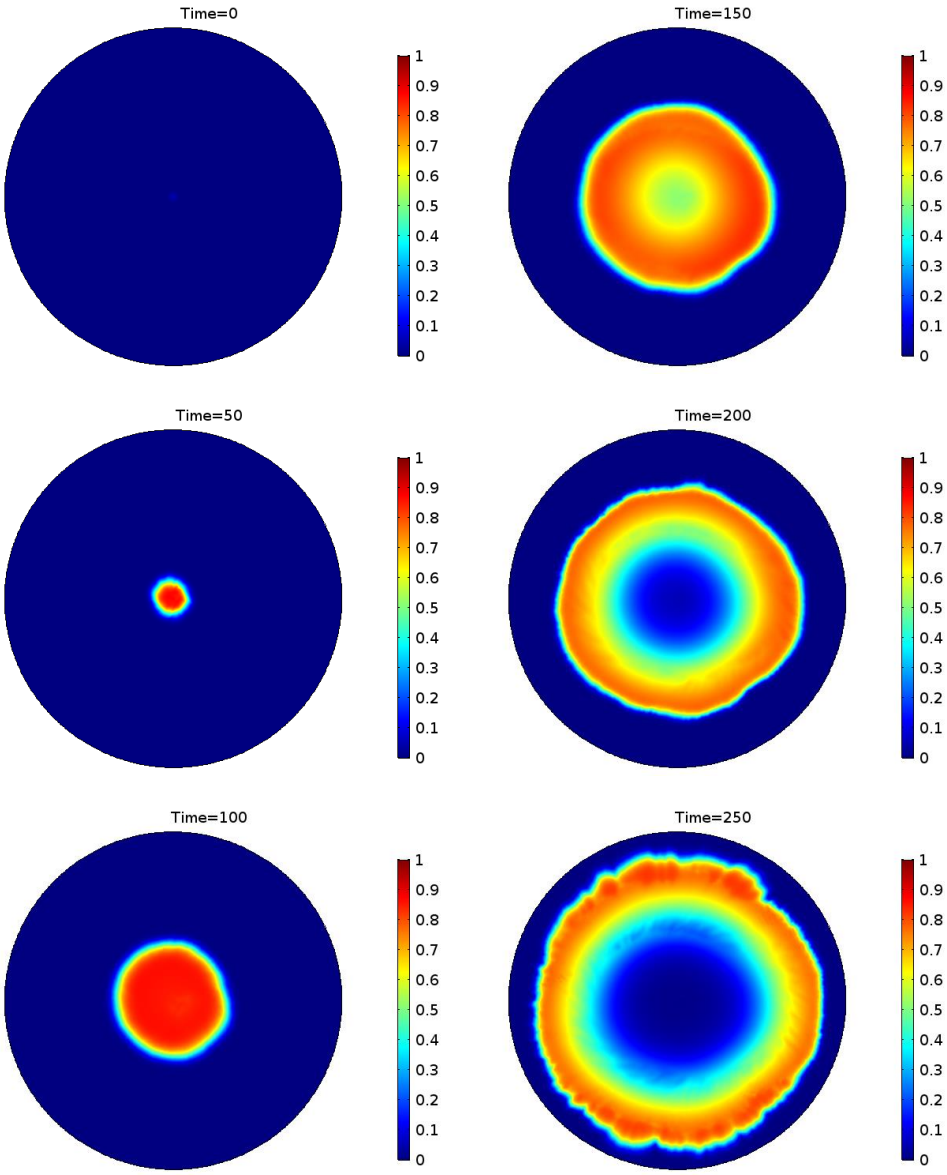

Figure 4.21: Sum of CSCs and normal tumor cells volumetric ratios for the basic Noisy Bell CSCs' initial distribution study

Compared to Fig.4.6, the ends of the proliferating zone (the outer part of the three-zone model) are outer distributed in Fig.4.21.

The performance of each phase in the evolution of dimensionless time has been quantified using Fig.4.22.

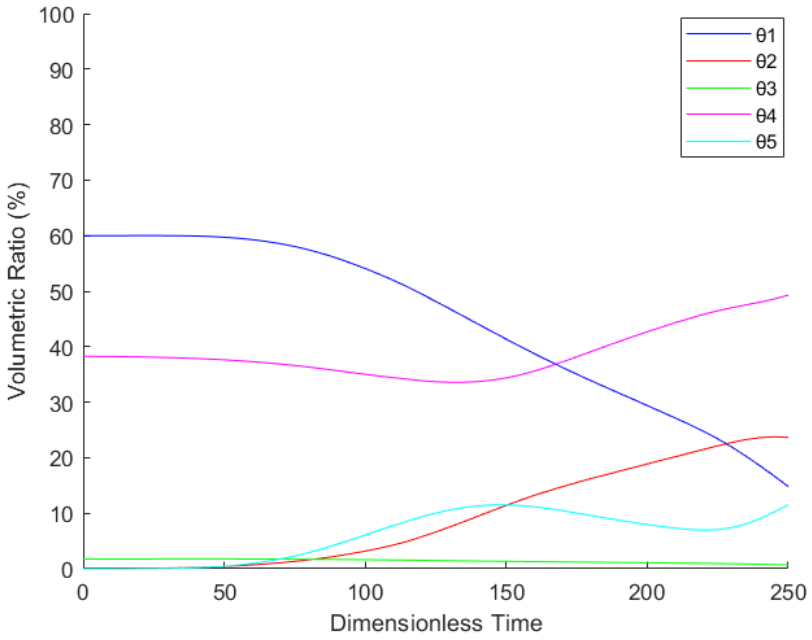

Figure 4.22: All phases and the nutrient's volumetric ratio, as simulation dimensionless time evolves, for the basic Noisy Bell CSCs' initial distribution study

The results are of the same nature, but normal tumor cells and CSCs are in higher volumetric ratios. As the phenomena progesses, oxygen levels drop and ECM levels rise, as dead cell waste builds up in the tumorous area. Healthy cells deplete as well. The three zones (necrotic, quiescent and proliferating) are being attempted to be defined in the following set of figures (Fig.4.23, 4.24, 4.25). As in Chapter 4.2., for 6 dimensionless times (0 , 50 , 100, 150, 200, 250) the 6 lines in Fig.4.23 (increasing in peak volumetric ratio as dimensionless time increases), showcase the blood vessels phase volumetric ratio, as a function of the radius of the studied region:

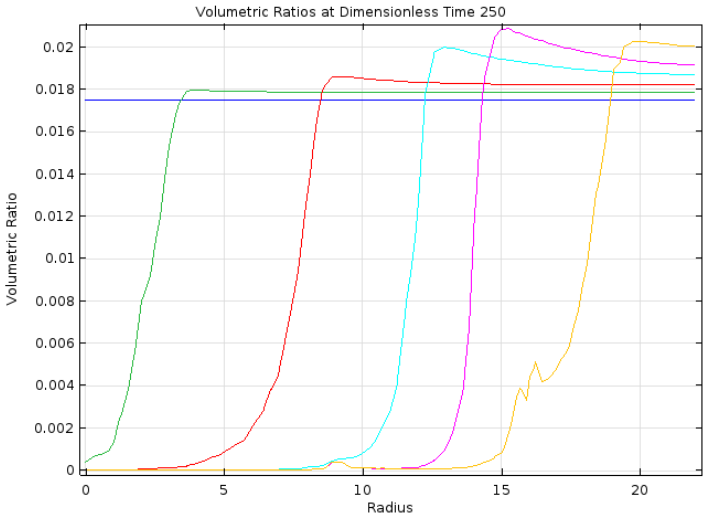

Figure 4.23: Blood vessels phase volumetric ratios as radius increases, for the basic Noisy bell CSCs' initial distribution study

In Fig.4.23, from radius 8.5 (by approximation) and onward for dimensionless time 250, the blood vessels phase has a local minimum, then has a minimal volumetric ratio until approximately radius 13.5 (which is shown in the orange line in Fig. 4.23 and the blue line in Fig.4.24 for the same dimensionless time), before beginning to increase until radius 19, when it is at its maximum. Fig.4.24 also illustrates the bare minimum volumetric ratio of the blood vessels phase before radius 8.5.

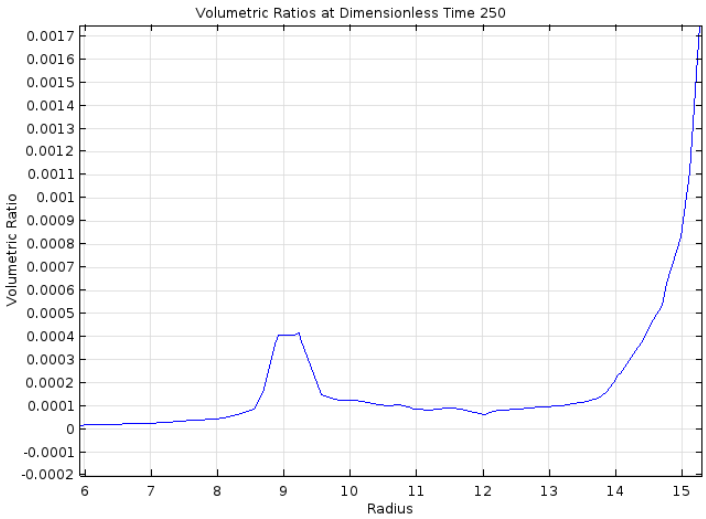

Figure 4.24: Enlarged blood vessels phase volumetric ratios diagram as radius increases, for the basic Noisy bell CSCs' initial distribution study

Following that point, the blood vessels phase remains quite steady. According to this information, there is a necrotic core up to radius 13 of the final dimensionless time. The accompanying figure (Fig.4.25) can help locate the quiescent and proliferating zones.

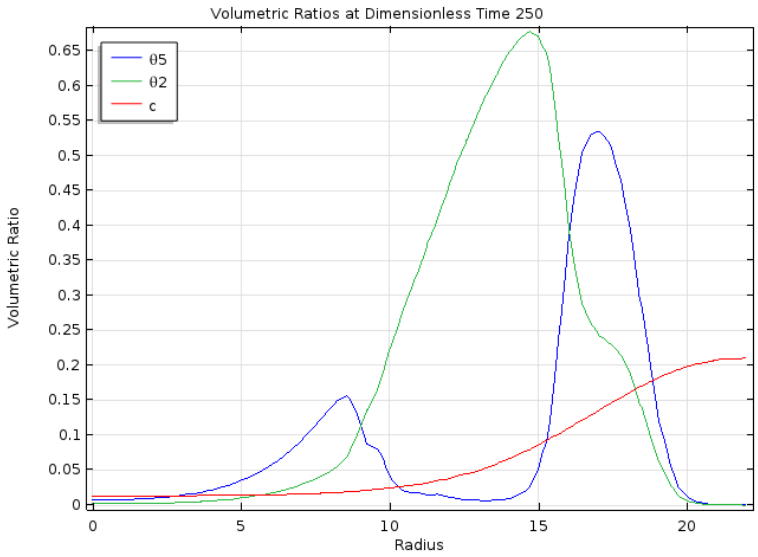

Figure 4.25: Normal tumor cells, CSCs and nutrient volumetric ratios as radius increases, for the basic Noisy bell CSCs' initial distribution study

According to figure 4.25, normal tumor cells proliferate approximately up to radius 15, at which point they abruptly start to drop. Approximately in radius 18, CSCs reach their peak volumetric ratio at the same time and subsequently start to deplete similarly to other tumor cells. The end of the proliferating zone, according to this diagram, appears to be at radius 20, which means that the quiescent and proliferating zones are in the radius range of (8.5, 20).

4.3.2. A Parametric Study on Noisy bell CSCs Distribution

The second parametric analysis used the identical data as the first in Chapter 4.2.2. ($k_{12}^{*} = 1.5$ as well), but the initial distribution of CSCs was noisy bell. The same format as before is used to present the results.

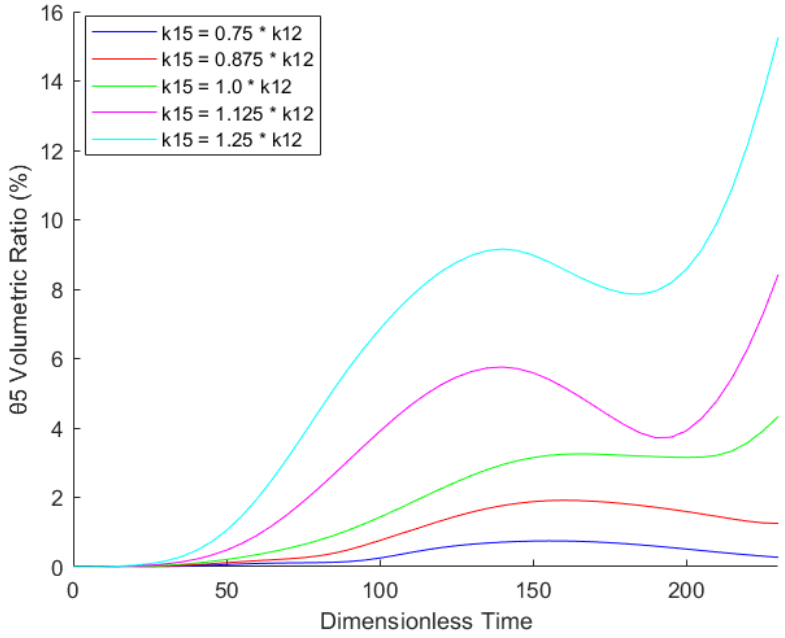

Figure 4.26: Cancer stem cells Volumetric ratios for different k_{15} values, and k_{25} = 0.8 * k_{22} (parametric study for Noisy Bell CSCs' initial distribution)

This time, as shown in Fig. 4.26, all CSCs end dimensionless time volumetric ratios are comparable, in contrast to the bell study. The final volumetric ratios of CSCs for each simulation were:

- For $k_{15} = 0.75 * k_{12}$: 0,27 %
- For $k_{15} = 0.875 * k_{12}$: 1,25 %
- For $k_{15} = 1.0 * k_{12}$: 4,32%
- For $k_{15} = 1.125 * k_{12}$: 8,43%
- For $k_{15} = 1.25 * k_{12}$: 15,26%

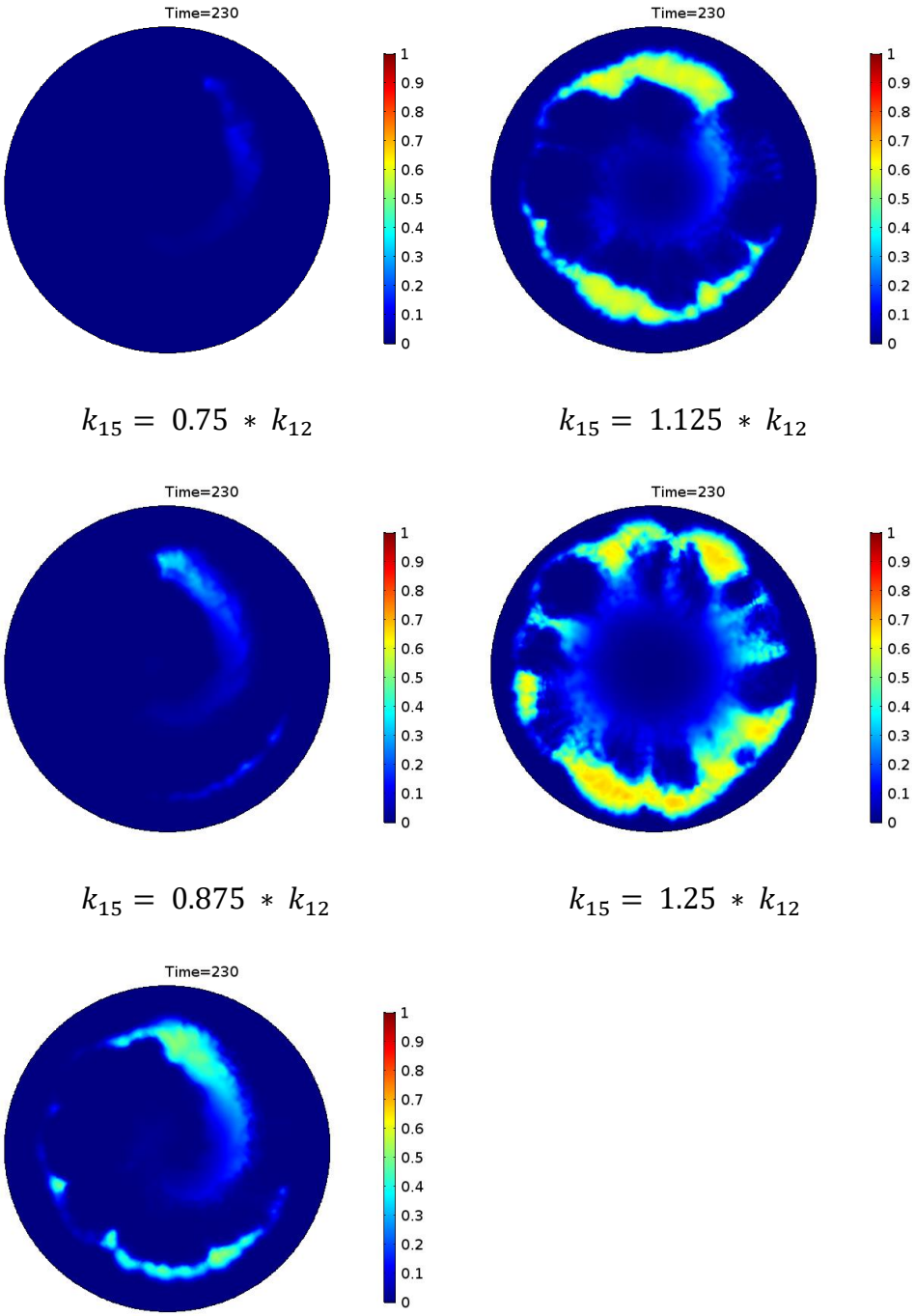

Figure 4.27: Snapshots of CSCs volumetric ratios in the final showcased time for each case (parametric study for Noisy Bell CSCs' initial distribution)

The necrotic core of the tumor, as is seen in the snapshots of Fig.4.27, contains a concentration of CSCs. As the simulation progresses, the whole CSCs phase shifts away

from the necrotic core and towards quiescent or proliferating regions. That is made clear in the two last simulations ($k_{15} = 1.125 * k_{12}$, $k_{15} = 1.25 * k_{12}$), where the phenomenon progresses more rapidly, and CSCs are missing from the necrotic core.

It is true so, that for noisy bell distribution of CSCs, $k_{15} = 1.125 * k_{12}$ or $k_{15} = 1.25 * k_{12}$ and $k_{25} = 0.8 * k_{22}$ and δ =0.9 , and final dimensionless time set to 250, CSCs are in accordance with the scientific data. Based on the evolution of the model, it is safe to say that for $k_{15} = 1.0 * k_{12}$, $k_{15} = 1.125 * k_{12}$, $k_{15} = 1.25 * k_{12}$ and the aforementioned parameters, CSCs will move out from the necrotic core completely, but higher dimensionless final time is needed.

5. Comments, Conclusions and Future Work

5.1. Some Comments on the two Basic studies

For the 2 basic studies (basic Bell and basic Noisy Bell, Chapters 4.2.1. and 4.3.1.), it is interesting to notice the difference between the volumetric ratio evolution of normal tumor cells and CSCs, as dimensionless time gets higher. The relevant graphs to illustrate such phenomena are provided below in Fig.5.1 and Fig.5.2:

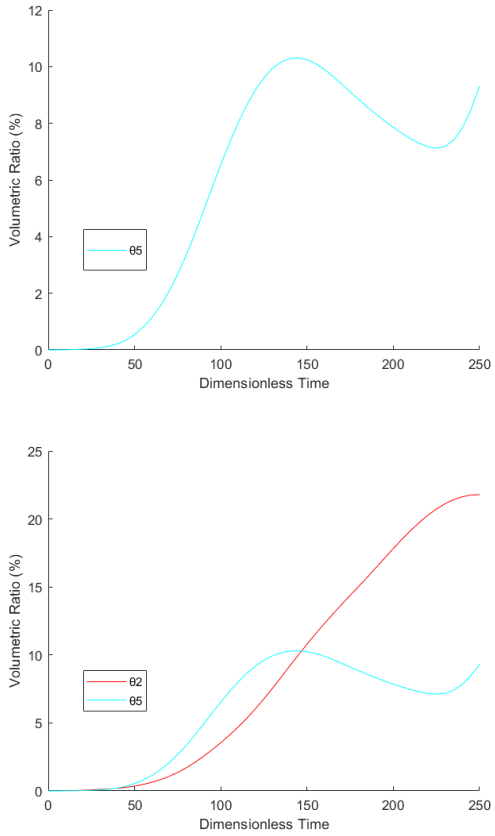

Figure 5.1: Upper Diagam: CSCs volumetric ratio for the basic Bell Study, Lower Diagram: Volumetric ratio of CSCs and Normal Tumor Cells for the basic Bell Study

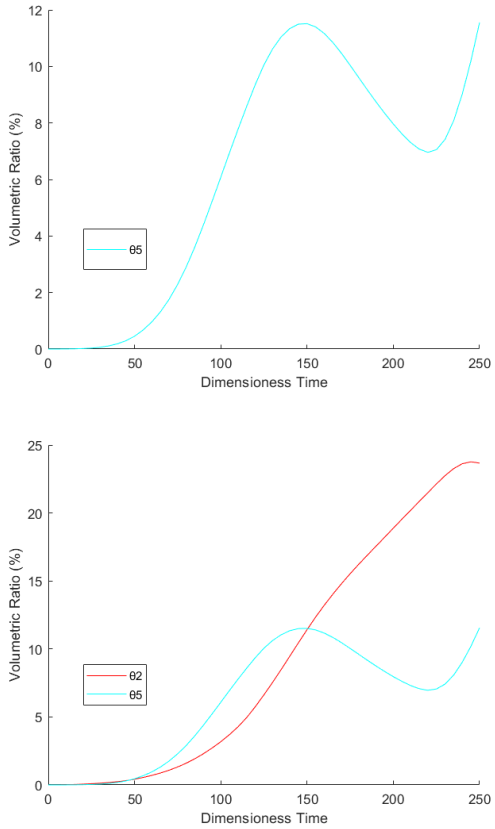

Figure 5.2: Upper Diagram: CSCs volumetric ratio for the basic Noisy Bell Study Lower Diagram: Volumetric ratio of CSCs and Normal Tumor Cells for the basic Noisy Bell Study

It is clear from both figures (Fig. 5.1, 5.2) that normal tumor cells monotonically increase as dimensionless time increases. There is a local peak in CSCs volumetric ratio approximately in dimensionless time 150, after which there is a decrease, and then a peak again of the same height at dimensionless time 250. The mobility of CSCs positions inside the research is what causes these phenomena. The niches eventually relocate to hypoxic or proliferating regions. By observing the simulations at dimensionless time 150, it is evident that CSCs are completely relocating away from the necrotic core, because of nutrient deprivation, which causes a part of them to experience cell death. The final volumetric ratio of CSCs (at dimensionless time 250) is 9,32% for bell initial CSCs distribution, and 11,55% for noisy bell initial CSCs distribution, which is a totally acceptable percentage. The final volumetric ratio of normal tumor cells is 21,79% for bell initial CSCs distribution, and for 23,67% noisy bell

initial CSCs distribution. The evolution of $\frac{\theta_5}{\theta_2}$ volumetric ratios ratio, is depicted in the figure below (Fig.5.3):

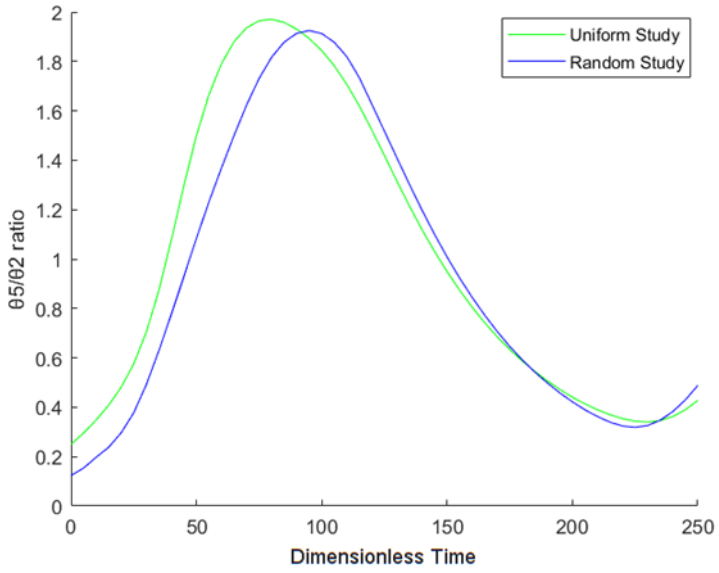

Figure 5.3: $\frac{\theta_5}{\theta_2}$ volumetric ratios ratio comparison between the basic Bell and the basic Noisy Bell study

CSCs are expressed in slightly larger quantities as a fraction of the volumetric ratio of normal tumor cells in general, except for the very end of the simulation dimensionless time.

In Chapters 4.2.1. and 4.3.1, it has been mentioned that the Noisy Bell CSCs distribution study, has some differences in θ_1, θ_3, θ_4 and nutrient volumetric fractions as well. This is going to be proved in the following diagrams (Fig. 5.4, 5.5, 5.6, 5.7).

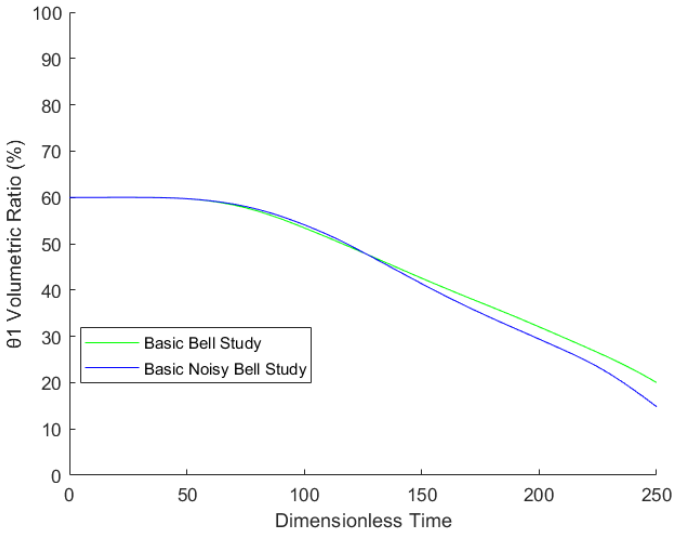

Figure 5.4: θ_1 volumetric ratios comparison between the basic Bell and the basic Noisy Bell study

In Fig.5.4, showing the comparison between healthy cells' volumetric ratio in both basic studies, healthy cells are slightly more depleted in Noisy Bell basic study, in the end dimensionless time. That is something that was evident by observing Fig.4.1 and 4.16. In the same tendency, θ_3 and nutrient are in lower volumetric ratios in the final dimensionless time, due to higher concentrations of tumor cells (normal and CSCs). The proof is in figure 5.5:

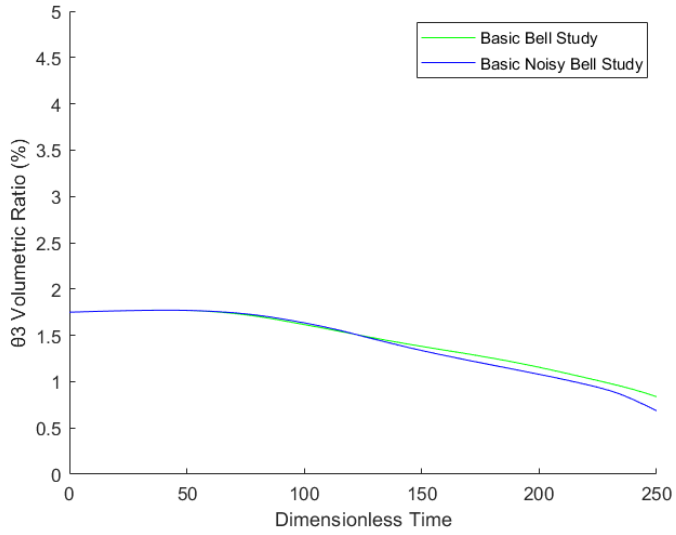

Figure 5.5: θ_3 volumetric ratios comparison between the basic Bell and the basic Noisy Bell study

Last comes the ECM phase diagram, which follows the oppossite tendency, a higher concentration in Noisy Bell CSCs distribution, in the final dimensionless time. That is because a slightl higher concentration in tumor cells dictates higher cellular waste, especially from dead heathy cells. The comparison is shown in Fig.5.7:

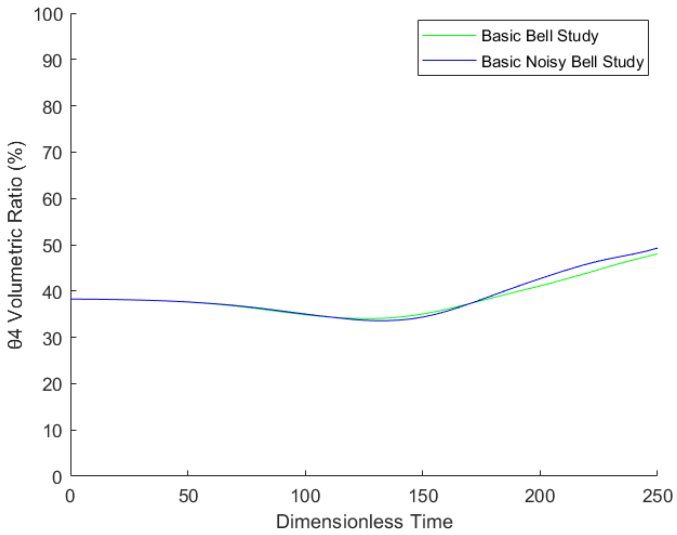

Figure 5.6: θ_4 phase volumetric ratios comparison between the basic Bell and the basic Noisy Bell study

As for conclusion, both basic studies are accurate in all necessary respects. The intention was to clarify which growth and death rates can be used for CSCs modeling. The combination of parameters presented in Chapters 4.2.1. and 4.2.2. can be used safely for modeling CSCs inside a 2D modelled vascular tumor.

5.2. Some comments on the Bell and the Noisy Bell parametric studies

As mentioned in Chapters 4.2.2. and 4.3.2., the cases which represent best the CSCs existence inside a tumorous region are:

- $k_{15} = 1.0 * k_{12}$, for Bell CSCs distribution
- $k_{15} = 1.125 * k_{12}$, for Bell CSCs distribution
- $k_{15} = 1.25 * k_{12}$, for Bell CSCs distribution
- $k_{15} = 1.125 * k_{12}$, for Noisy Bell CSCs distribution
- $k_{15} = 1.25 * k_{12}$, for Noisy Bell CSCs distribution

In all cases, $k_{25} = 0.8 * k_{22}$, δ = 0.9, k_{12}^*= 2.0, final dimensionless time is set to 230 and radius is set to 22.

All in-between k_{15}^* values can be also used, i.e., all k_{15}^* values in the spectrum $k_{15} = (1.0 , 1.25) * k_{12}$ for Bell CSCs distribution and all k_{15}^* values in the spectrum $k_{15} = (1.125 , 1.25) * k_{12}$ for Noisy Bell CSCs distribution, for the same values used in all the other parameters.

It is of great interest to show as well which CSCs' growth and death rates do not fit the range of needed parameters to fit scientific data. When the CSCs initial distribution is bell, and $k_{15} = 1.0 * k_{12}$, or lower, the results are not corresponding to the data for CSCs existence. It is emphasized that this is not the case in every situation where such growth rates are used. This is accurate when:

- δ = 0.9 or lower, and
- $k_{25} = 0.8 * k_{22}$ or higher, and
- k_{12}^*= 1.5 or lower.
- Dimensionless time is set to the range (0, 230). If it is set to increased amounts of upper value, then the radius of the circular studied region must get higher in value (more than 22), so the simulated tumor cells do not reach or exceed the domain's boundaries.

5.3. Conclusions and Future Work

The goal of this thesis was the successful incorporation of CSCs in the mass balance and momentum balance equations of cellular phases, as well as in the reaction – diffusion equations of the chemical species (oxygen). What is more, it was needed to showcase a set of simulations that are in accordance with the scientific data for the 2 basic hypotheses of CSCs' existence inside the tumor: a valid range of volumetric ratios, and CSCs outside of the necrotic core.

By achieving this goal, not only a successful modeling represented scientific reality, but also a valid range of proliferation rates of CSCs, in combination with a fixed value for the CSCs' death rate was evaluated.

This thesis can serve as the foundation for future work concerning extension of CSCs modeling in tumors. Specifically, finding a valid range of death rates of CSCs (instead of a fixed death rate of CSCs) in combination with a valid range of proliferation rates of the aforementioned phase, can expand the capabilities of tumor modeling. Expanding this model in a model that contains more phases, or even more sub-phases (e.g., young vessels, mature vessels) is also possible.

Lastly, it would be a success for this thesis, if the results presented here, can guide a researcher to incorporate CSCs in cancer therapy modeling. Either in conventional therapies, or in more specified therapies, such as Car-T Cell therapy, expanding the existing equations is now easier, having already modeled how CSCs are existing inside a vascular growing tumor.

6. Bibliography

[1] M. E. Hubbard and H. M. Byrne, 'Multiphase modelling of vascular tumour growth in two spatial dimensions', 2012, doi: 10.1016/j.jtbi.2012.09.031.

[2] P. Anand *et al.*, 'Expert Review Cancer is a Preventable Disease that Requires Major Lifestyle Changes', 2008, doi: 10.1007/s11095-008-9661-9.

[3] N. V. Yaglova, E. P. Timokhina, S. S. Obernikhin, and V. V. Yaglov, 'Emerging Role of Deuterium/Protium Disbalance in Cell Cycle and Apoptosis', *Int J Mol Sci*, vol. 24, no. 4, Feb. 2023, doi: 10.3390/IJMS24043107.

[4] G. M. Cooper, 'The Cell', vol. 8, pp. 103–108, 2000, Accessed: Sep. 25, 2023. [Online]. Available: https://www.ncbi.nlm.nih.gov/books/NBK9839/

[5] 'Cytogenetics Gallery'. Accessed: Sep. 25, 2023. [Online]. Available: http://www.pathology.washington.edu/galleries/cytogallery/main.php?file=what%20is%20a%20chromosome

[6] S. M. Mallya and P. Diplomate, 'White and Pharoah's Oral Radiology: Principles and Interpretation - Sanjay Mallya, Ernest Lam - 8th Edition (2018) 1608 pp., ISBN: 9780323543842', 2018.

[7] J. A. Waters and C. D. House, 'Ovarian cancer stem cell biology and chemoresistance', in *Overcoming Ovarian Cancer Chemoresistance*, Elsevier, 2020, pp. 55–77. doi: 10.1016/B978-0-12-819840-7.00009-1.

[8] G. Bussolati, C. Marchiò, L. Gaetano, R. Lupo, and A. Sapino, 'Pleomorphism of the nuclear envelope in breast cancer: A new approach to an old problem', *J Cell Mol Med*, vol. 12, no. 1, pp. 209–218, Jan. 2008, doi: 10.1111/J.1582-4934.2007.00176.X.

[9] S. Hamouda, R. El-Ezz, and M. E. Wahed, 'Enhancement Accuracy of Breast Tumor Diagnosis in Digital Mammograms', *J Biomedical Sci*, vol. 2017, no. 4, p. 28, 2017, doi: 10.4172/2254-609X.100072.

[10] Y. Cui, Y. Li, D. Xing, T. Bai, J. Dong, and J. Zhu, 'Improving the Prediction of Benign or Malignant Breast Masses Using a Combination of Image Biomarkers and Clinical Parameters', *Front Oncol*, vol. 11, p. 629321, Mar. 2021, doi: 10.3389/FONC.2021.629321.

[11] M. Saraiya *et al.*, 'US Assessment of HPV Types in Cancers: Implications for Current and 9-Valent HPV Vaccines', *JNCI Journal of the National Cancer Institute*, vol. 107, no. 6, Jun. 2015, doi: 10.1093/JNCI/DJV086.

[12] F. Huang, B. Pan, J. Wu, E. Chen, and L. Chen, 'Relationship between exposure to PM2.5 and lung cancer incidence and mortality: A meta-analysis', *Oncotarget*, vol. 8, no. 26, p. 43322, Jun. 2017, doi: 10.18632/ONCOTARGET.17313.

[13] 'The Genetics of Cancer - NCI'. Accessed: Sep. 25, 2023. [Online]. Available: https://www.cancer.gov/about-cancer/causes-prevention/genetics

[14] S. O. Dalton, E. H. Boesen, L. Ross, I. R. Schapiro, and C. Johansen, 'Mind and cancer: Do psychological factors cause cancer?', *Eur J Cancer*, vol. 38, no. 10, pp. 1313–1323, Jul. 2002, doi: 10.1016/S0959-8049(02)00099-0.

[15] L. A. van Tuijl *et al.*, 'Psychosocial factors and cancer incidence (PSY-CA): Protocol for individual participant data meta-analyses', *Brain Behav*, vol. 11, no. 10, Oct. 2021, doi: 10.1002/BRB3.2340.

[16] D. Hanahan and R. A. Weinberg, 'The Hallmarks of Cancer', *Cell*, vol. 100, no. 1, pp. 57–70, Jan. 2000, doi: 10.1016/S0092-8674(00)81683-9.

[17] T. Gutschner and S. Diederichs, 'The hallmarks of cancer: A long non-coding RNA point of view', *RNA Biol*, vol. 9, no. 6, p. 703, Jun. 2012, doi: 10.4161/RNA.20481.

[18] J. Groten, A. Venkatraman, and R. Mertelsmann, 'Modeling and Simulating Carcinogenesis', *Precision Medicine: Tools and Quantitative Approaches*, pp. 277–295, Jan. 2018, doi: 10.1016/B978-0-12-805364-5.00012-3.

[19] T. B. Steinbichler *et al.*, 'Cancer stem cells and their unique role in metastatic spread', *Semin Cancer Biol*, vol. 60, pp. 148–156, Feb. 2020, doi: 10.1016/J.SEMCANCER.2019.09.007.

[20] D. Hanahan and R. A. Weinberg, 'Hallmarks of cancer: The next generation', *Cell*, vol. 144, no. 5, pp. 646–674, Mar. 2011, doi: 10.1016/J.CELL.2011.02.013/ATTACHMENT/68024D79-3A9C-46C4-930B-640934F11E2E/MMC1.PDF.

[21] V. Adorno-Cruz *et al.*, 'Cancer Stem Cells: Targeting the Roots of Cancer, Seeds of Metastasis, and Sources of Therapy Resistance', *Cancer Res*, vol. 75, no. 6, p. 924, Mar. 2015, doi: 10.1158/0008-5472.CAN-14-3225.

[22] Y. Song *et al.*, 'A unified model of the hierarchical and stochastic theories of gastric cancer', *Br J Cancer*, vol. 116, no. 8, p. 973, Apr. 2017, doi: 10.1038/BJC.2017.54.

[23] W. Yin, J. Wang, L. Jiang, and Y. James Kang, 'Cancer and stem cells', *Experimental Biology and Medicine*, vol. 246, no. 16. SAGE Publications Inc., pp. 1791–1801, Aug. 01, 2021. doi: 10.1177/15353702211005390.

[24] V. Plaks, N. Kong, and Z. Werb, 'The cancer stem cell niche: how essential is the niche in regulating stemness of tumor cells?', *Cell Stem Cell*, vol. 16, no. 3, pp. 225–238, Mar. 2015, doi: 10.1016/J.STEM.2015.02.015.

[25] H. Zhong, S. Brown, S. Devpura, X. A. Li, and I. J. Chetty, 'Kinetic modeling of tumor regression incorporating the concept of cancer stem-like cells for patients with locally advanced lung cancer', 2018, doi: 10.1186/s12976-018-0096-7.

[26] I. Baccelli and A. Trumpp, 'The evolving concept of cancer and metastasis stem cells', *Journal of Cell Biology*, vol. 198, no. 3, pp. 281–293, Aug. 2012, doi: 10.1083/jcb.201202014.

[27] H. Zhou, L. Tan, B. Liu, and X. Y. Guan, 'Cancer stem cells: Recent insights and therapies', *Biochem Pharmacol*, vol. 209, p. 115441, Mar. 2023, doi: 10.1016/J.BCP.2023.115441.

[28] ‘Cancer Stem Cells Theory - EuroStemCell Research’. Accessed: Sep. 25, 2023. [Online]. Available: https://www.eurostemcell.org/cancer-disease-stem-cells

[29] A. Bradshaw, A. Wickremsekera, S. T. Tan, L. Peng, P. F. Davis, and T. Itinteang, ‘Cancer Stem Cell Hierarchy in Glioblastoma Multiforme’, *Front Surg*, vol. 3, p. 1, Apr. 2016, doi: 10.3389/FSURG.2016.00021.

[30] T. Lapidot *et al.*, ‘A cell initiating human acute myeloid leukaemia after transplantation into SCID mice’, *Nature 1994 367:6464*, vol. 367, no. 6464, pp. 645–648, 1994, doi: 10.1038/367645a0.

[31] N. Terraneo, F. Jacob, A. Dubrovska, and J. Grünberg, ‘Novel Therapeutic Strategies for Ovarian Cancer Stem Cells’, *Front Oncol*, vol. 10, p. 319, Mar. 2020, doi: 10.3389/FONC.2020.00319.

[32] Y. Liu, M. Yang, J. Luo, and H. Zhou, ‘Radiotherapy targeting cancer stem cells “awakens” them to induce tumour relapse and metastasis in oral cancer’, *International Journal of Oral Science 2020 12:1*, vol. 12, no. 1, pp. 1–12, Jun. 2020, doi: 10.1038/s41368-020-00087-0.

[33] M. P. Deonarain, C. A. Kousparou, and A. A. Epenetos, ‘Antibodies targeting cancer stem cells: A new paradigm in immunotherapy?’, *MAbs*, vol. 1, no. 1, p. 12, Jan. 2009, doi: 10.4161/MABS.1.1.7347.

[34] ‘CAR T Cells: Engineering Immune Cells to Treat Cancer - NCI’. Accessed: Sep. 25, 2023. [Online]. Available: https://www.cancer.gov/about-cancer/treatment/research/car-t-cells

[35] Y. Arima, H. Nobusue, and H. Saya, ‘Targeting of cancer stem cells by differentiation therapy’, *Cancer Sci*, vol. 111, no. 8, p. 2689, Aug. 2020, doi: 10.1111/CAS.14504.

[36] K. Gairola, S. Gururani, A. Bahuguna, V. Garia, R. Pujari, and S. K. Dubey, ‘Natural products targeting cancer stem cells: Implications for cancer chemoprevention and therapeutics’, *J Food Biochem*, vol. 45, no. 7, Jul. 2021, doi: 10.1111/JFBC.13772.

[37] I. G. Gonçalves and J. M. García-Aznar, ‘Hybrid computational models of multicellular tumour growth considering glucose metabolism’, *Comput Struct Biotechnol J*, vol. 21, p. 1262, Jan. 2023, doi: 10.1016/J.CSBJ.2023.01.044.

[38] A. Rivaz, M. Azizian, and M. Soltani, ‘Various Mathematical Models of Tumor Growth with Reference to Cancer Stem Cells: A Review’, *Iran J Sci Technol Trans A Sci*, vol. 43, no. 2, pp. 687–700, Apr. 2019, doi: 10.1007/S40995-019-00681-W.

[39] S. Dini *et al.*, ‘Identifying the necrotic zone boundary in tumour spheroids with pair-correlation functions’, 2016, doi: 10.1098/rsif.2016.0649.

[40] J. P. Ward and J. R. King, ‘Mathematical modelling of avascular-tumour growth’, *Math Med Biol*, vol. 14, no. 1, pp. 39–69, Mar. 1997, doi: 10.1093/IMAMMB/14.1.39.

[41] C. J. W. Breward, H. M. Byrne, and C. E. Lewis, ‘A multiphase model describing vascular tumour growth’, *Bull Math Biol*, vol. 65, no. 4, pp. 609–640, 2003, doi: 10.1016/S0092-8240(03)00027-2.

[42] P. Macklin and M. E. Edgerton, 'Discrete cell modeling', *Multiscale Modeling of Cancer: An Integrated Experimental and Mathematical Modeling Approach*, vol. 9780521884426, pp. 88–122, Jan. 2010, doi: 10.1017/CBO9780511781452.007.

[43] K. A. Rejniak and A. R. A. Anderson, 'Hybrid Models of Tumor Growth', *Wiley Interdiscip Rev Syst Biol Med*, vol. 3, no. 1, p. 115, Jan. 2011, doi: 10.1002/WSBM.102.

[44] A. Rivaz, M. Azizian, and M. Soltani, 'Various Mathematical Models of Tumor Growth with Reference to Cancer Stem Cells: A Review', *Iran J Sci Technol Trans A Sci*, vol. 43, no. 2, pp. 687–700, Apr. 2019, doi: 10.1007/S40995-019-00681-W.

[45] I. Lampropoulos, M. Charoupa, and M. Kavousanakis, 'Intra-tumor heterogeneity and its impact on cytotoxic therapy in a two-dimensional vascular tumor growth model', *Chem Eng Sci*, vol. 259, p. 117792, Sep. 2022, doi: 10.1016/J.CES.2022.117792.

[46] 'Choosing the Right Linear System Solver'. Accessed: Sep. 26, 2023. [Online]. Available: https://doc.comsol.com/5.5/doc/com.comsol.help.comsol/comsol_ref_solver.27.118.html

7. Figures Table